INVESTIGATION OF MICROSTRIP PATCH ANTENNA USING COMPLEMENTARY SPLIT RING RESONATORS FOR WIRELESS APPLICATIONS

A thesis submitted in partial fulfilment of the requirements
for the award of degree of

MASTER OF ENGINEERING
In
Wireless Communication

Submitted By
Smriti
Roll No. 801263026

Under guidance of
Ms. Jaswinder Kaur
Lecturer, ECED

Department of Electronics and Communication Engineering
THAPAR UNIVERSITY, PATIALA-147004
PUNJAB (INDIA)

July 2014

CERTIFICATE

I hereby declare that the work which is being presented in the thesis entitled, **"Investigation of Microstrip patch antenna Using Complementary Split Ring Resonators For Wireless Applications"** in partial fulfilment of the requirement for the award of degree of M.E in Wireless Communication submitted in Electronics and Communication Engineering Department of Thapar University, Patiala is an authentic record of my own work carried out under the supervision of Ms. Jaswinder Kaur, Lecturer, ECED, Thapar University, Patiala.

The matter presented in this thesis has not been submitted in any other University/Institute for the award of degree.

Smriti

(SMRITI)

ROLL NO: 801263026

Date: 15/07/2014

It is certified that the above statement made by the student is correct to the best of my knowledge and belief.

Jaswinder Kaur 15/07/14

(Mrs. Jaswinder Kaur)
Lecturer
ECED, Thapar University
Patiala, 147004

Countersigned By:-

Dr. Sanjay Sharma
Professor & Head
ECED, Thapar University
Patiala, 147004

Dr. S.K. Mohapatra
Dean of Academic Affairs
Thapar University
Patiala, 147004

ACKNOWLEDGEMENT

To discover, analyse and to present something new is to venture on an untraded path towards and unexplored destination is an arduous adventure unless one gets a true torch bearer to show the way. I would have never succeeded in completing my task without the cooperation, encouragement and help provided to me by various people. Words are often too less to reveals one's deep regards. I take this opportunity to express my profound sense of gratitude and respect to all those who helped me through the duration of this thesis. I acknowledge with gratitude and humility my indebtedness to **Ms. Jaswinder Kaur, Lecturer,** Electronics and Communication Engineering Department, Thapar University, Patiala, under whose guidance I had the privilege to complete this thesis. I wish to express my deep gratitude towards her for providing individual guidance and support throughout the thesis work.

I convey my sincere thanks to **Professor & Head of the Department, Dr. Sanjay Sharma** as well as **PG Coordinator, Dr. Kulbir Singh, Associate Professor,** Electronics and Communication Engineering Department, entire faculty and staff of Electronics and Communication Engineering Department for their encouragement and cooperation.

My greatest thanks are to all who wished me success especially my parents. Above all I render my gratitude to the Almighty who bestowed self-confidence, ability and strength in me to complete this work for not letting me down at the time of crisis and showing me the silver lining in the dark clouds. I do not find enough words with which I can express my feelings of thanks to my dear friends for their help, inspiration and moral support which went a long way in successful competition of the present study.

(Smriti)

ABSTRACT

Microstrip has emerged as the most revolutionary antenna technology ever. Microstrip patch antennas (MPAs) are preferred over other antennas in today's scenario for their compatibility to be fit in mobile, aircraft, satellites owing to very small sizes. Hence design and development of superior and cost effective MPAs has become an active research area. Moreover, considerable development work in the field of MPAs has been going on in trying to meet the increasingly demanding systems requirements such as size miniaturization, improved bandwidth, multifrequency operations etc.

This thesis work focuses mainly on design and analysis of MPA using metamaterial. Metamaterials are the artificial materials engineered to impart properties which may not be easily procurable in nature. These materials generally inherit their properties from structure instead of composition, utilizing the inclusion of slight inhomogeneities to accomplish effective macroscopic behaviour. The metamaterial used in this thesis work is Complementary Split Ring Resonator (CSRR). A CSRR is a highly conductive structure in which the capacitance between the two rings balances its inductance. When time-varying electric field is applied parallel to the rings surface, it induces currents which, in dependence on the resonant properties of the structure, produce a magnetic field that may either oppose or enhance the incident field, thus resulting in positive or negative effective ϵ. The presented work includes designing and simulation of two designs, one having coplanar rectangular MPAs with slotted CSRR in the ground plane and other without slotted CSRR. The effect of CSRR inclusion on different parameters such as return loss, bandwidth and mutual coupling has been studied. The simulation results confirm that slotted CSRR shows significant reduction of return loss along with improvement in the bandwidth. In addition, reduction in the mutual coupling between two antenna elements has been observed, thereby making the structure suitable for minimizing coupling and co-channel interference in multiband antennas. The research work also includes simulation of a dual band MPA with two side-by-side CSRR structures on a single patch fed by a microstrip line covering the two WLAN bands in 2.4 (2.4–2.484 GHz) and 5.2 (5.15–5.35 GHz). The dimensions of the complementary ring elements as well as microstrip feed-line width have been varied for required resonant frequencies and return loss characteristics. Simulated results including current distribution and radiation pattern have been analysed. This design has been extended for a multiband MPA which consists of two open-circuited stubs added on each side of the antenna along

with two side-by-side CSRR structures on a single patch. The suggested antenna finds applications in various wireless systems since it covers different IEEE standards which include WLAN bands in 2.4 (2.4–2.484 GHz) and 5.8 (5.725–5.825 GHz), Bluetooth (2.4-2.5 GHz) and WiMAX bands of (2.5-2.69 GHz and 5.25-5.85 GHz) and X-band satellite downlink (7.25 GHz-7.75 GHz).. The designed antenna has been simulated using the commercially available software CST Microwave Studio 2010. With the help of the simulated results, various parameters like return loss, gain, directivity, VSWR and bandwidth have been discussed. The multiband antenna has been fabricated and the fabricated antenna has been tested in VNA (Vector Network Analyser). Finally, the simulated results have been compared with measured results obtained from the fabricated antenna.

TABLE OF CONTENTS

LIST OF FIGURES

LIST OF TABLES

LIST OF ABBREVIATIONS

CPW	Coplanar Waveguide
CST	Computer Simulation Technology
PCB	Printed Circuit Board
CSRR	Complementary Split Ring Resonators
IEEE	Institute of Electrical and Electronics Engineers
ISM	Industrial Scientific and Medical
LHMs	Left-Handed Metamaterials
MMICs	Microwave Monolithic Integrated Circuits
MPA	Microstrip Patch Antenna
RMPA	Rectangular Microstrip Patch Antenna
SRR	Split Ring Resonators
TEM	Tranverse Electric Magnetic
TM	Transverse Magnetic
VNA	Vector Network Analyser
WiFi	Wireless Fidelity
WLAN	Wireless Local Area Network
WiMAX	Worldwide Interoperability for Microwave Access

CHAPTER-1
INTRODUCTION

1.1. An Introduction to Wireless Communication

The term wireless communication is commonly used in telecommunications industry and refers to the telecommunications systems which utilizes some form of energy (e.g. radio waves, etc.) to convey information with no use of wires. Wireless operations allow various services, which include long-range communications that are unfeasible to execute with the use of wires. Information is transmitted in this mode across both short and long distances. The wireless technology has continuously been enhancing with time because of the following advantages:

- Communication has further improved the quality to transfer the information rapidly to the consumers.
- Working professionals can get hands on Internet whenever and wherever they go without carrying any cables or wires; thereby accomplishing the work on time and thus improving the productivity.
- Critical situation can be forewarned through wireless communication. The influenced regions can therefore be supported with help timely.
- Wireless networks are economical to install and manage.

Wireless technology has covered many evolutionary paths and has enhanced performance and efficiency in mobile environment. With every generation, there has been significant advancement in the performance of wireless technology. The first generation (1G) had accomplished the target of basic mobile voice and in the second generation (2G), the coverage and capacity were initiated. After these generations, third generation (3G) came into subsistence which improved the rate of data transfer in the broadband which will develop further in Fourth generation (4G).

WLAN and WiMAX technology is the most expeditiously developing field in the contemporary wireless communication since it permits the users the mobility within a broad coverage area besides being connected to the network, thereby supporting remarkably increased flexibility. Wireless has become favoured for the home user due to local freedom and ease of installation. Naturally, these applications demand antennas. This being the case, compact antenna technology has developed accompanied by mobile and cellular technologies. It is crucial to have the proper antenna for a device as it will

upgrade the transmission and reception, lower power consumption and boost the marketability of the communication device. Because of features like low cost, low profile, MPAs are well suited for WLAN/WiMAX application systems.

1.1.1. IEEE standard for WLAN

The IEEE 802.11 standard was proposed in 1997 for WLANs application. After few years, new standard was proposed, operating on the 2.4 GHz ISM band (2.4-2.484 GHz) which is called as 802.11b or 802.11HR (High Rate) providing data rate upto 11Mbps. The IEEE 802.11a standard was approved in 1999, operating on the 5GHz ISM bands (5.15-5.35GHz and 5.725-5.825GHz). The change of band shows that 802.11a and 802.11b products are not compatible, therefore, the IEEE proposed 802.11g standard which is compatible with both 802.11b and 802.11a technology. The 802.11g standard was accepted in 2003. Since 802.11b and 802.11g are using 2.4GHz frequency band while 802.11a uses 5GHz frequency band so a dual band antenna is required for WLAN applications. The popularity of WLAN is increased due to high-speed transfer rate [1].

1.1.2. IEEE standard for WiMAX

WiMAX technology is based upon IEEE 802.16 standard called as Broadband Wireless Access. The term WiMAX was coined by WiMAX forum which was established in June 2001 to upgrade interoperability and conformity of the standard. The forum defines WiMAX as “standards-based technology permitting the last mile wireless broadband access as a substitute to DSL”. There is no fixed global licensed spectrum for WiMAX, even though the WiMAX Forum has declared three licensed profiles of the spectrum: 2.5GHz (2.5-2.69 GHz), 3.5GHz (3.4-3.69 GHz) and 5.5GHz (5.25-5.85 GHz). WiMAX provides data rate upto 70 Mbps over 50 km. IEEE 802.16-2004 is often called IEEE 802.16d because that was the working party that advanced the standard. It is often called as “fixed WiMAX” since it offers no support for the mobility. It replaced IEEE Standards 802.16-2001, 802.16c-2002, and 802.16a-2003. 802.16e-2005 is an amendment to 802.16-2004 and is usually called as 802.16e. It presented the support for mobility, along with other things and is consequently called as “mobile WiMAX” [1].

1.2. Introduction to MPAs

Microstrip is probably the most successful and revolutionary antenna technology ever. Although introduced in the 1950's., this concept had to wait for about 20 years to be realized after the development of the Printed Circuit Board (PCB) technology in the 1970s. Since then, MPAs are the most common types of antennas with wide range of applications due to their following advantages:

- Light weight
- Easy and low cost fabrication
- Mechanical robustness
- Superior portability
- Planar
- Suitable for array with the ease of fabrication and integration with microwave monolithic integrated circuits (MMICs)
- Versatile in terms of electromagnetic characteristics (input impedance, radiation pattern, polarization).
- Since MPAs radiate a comparatively broad beam broadside to the plane of the substrate, therefore, these exhibit a low profile, and therefore can be fabricated employing printed circuit (photolithographic) techniques which means that the antenna can be modelled conformable, and possibly at low cost.

Disadvantages of the MPA configurations are as follows:

- The bandwidth attained is narrow.
- Radiation from the feeds contributes to the radiation pattern.
- The polarization purity is poor.
- The power capacity is limited along with some tolerance problems.

Considerable development work in the field of MPAs has been done in trying to deal with these problems, so as to assure increasingly demanding systems requirements. This endeavour has involved the advancement of novel MPA configurations and the evolution of meticulous and multifaceted analytical models for the apprehension of the inherent limitations of MPAs, along with their design and optimization.

1.2.1. Radiation mechanism of an MPA

Radiation from MPA can be intended from the distribution of field between the patch metalization and ground plane. Alternatively, radiation can be described in terms of the surface current distribution on the patch metalization.

Let us consider a MPA coupled to a microwave source. This results in energizing of the patch which will create distribution of +ve and –ve charges on the upper and lower surfaces of the patch along with the surface of the ground plane [3].

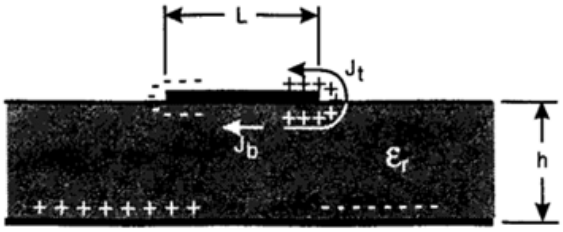

Figure 1.1. Distribution of charges and current density on a MPA [3]

This nature of the charge distribution occurs because of the fact that at the dominant mode, the patch is about a half-wave long. The repulsive forces existing between the similar charges over the bottom surface of the patch drift some charges around its edges, to its top surface. This flow of charges results in corresponding current densities $\overrightarrow{J_t}$ and $\overrightarrow{J_b}$ at the top and bottom surfaces of the patch as shown in the Figure 1.1. For most MPAs, the ratio of h/W (that is ratio of substrate thickness to patch width) is very small. Therefore, the attractive force existing between the charges dominates and most of the charge concentration and the flow of current persists under the patch. A small amount of current drifts through the patch edges to its top surface and is responsible for a weak magnetic field tangential to the patch edges. Thus, a simple approximation is made in which the tangential magnetic field is zero and magnetic walls can be placed all through the periphery of the patch. Since the substrate employed is quite thin in comparison to the wavelength ($h \ll \lambda$) in the dielectric, the field variations along the height can be considered to be constant and the electric field nearly normal to the surface of the patch. Consequently, the patch can be designed as a cavity having electric walls (since the electric field is normal to the surface of the patch) on the top and below along with four magnetic walls besides the patch edges (since the tangential magnetic field is extremely weak). Only TM modes are feasible in this cavity. The electric field distribution for the dominant TM_{100} mode of the cavity is shown in Figure 1.2.

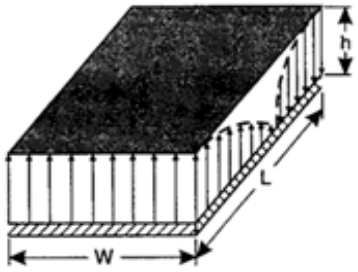

Figure 1.2. Electric field distribution in the microstrip cavity [3]

The four sidewalls of the cavity indicate four narrow apertures or slots through which radiation takes place. Using the Huygen field equivalence principle, the microstrip patch can be represented by an equivalent current density $\overrightarrow{J_t}$ at the top surface to account for the presence of patch metalization. The four side slots are represented by the equivalent current densities $\overrightarrow{J_s}$ and $\overrightarrow{M_s}$, corresponding to the magnetic and electric fields $\overrightarrow{H_a}$ and $\overrightarrow{E_a}$, respectively, the slots. The equivalent currents are shown in Figure 1.3(a) and are given by

$$\overrightarrow{J_s} = \hat{n} \times \overrightarrow{H_a} \tag{1.1}$$

$$\overrightarrow{M_s} = -\hat{n} \times \overrightarrow{E_a} \tag{1.2}$$

For thin substrates, it was shown that the patch current at the top $\overrightarrow{J_t}$ is much smaller than $\overrightarrow{J_b}$, the current at the bottom. It will be set to zero here to indicate negligible radiation from the patch current. Similarly, the tangential magnetic fields along the patch edges and the corresponding current density $\overrightarrow{J_s}$ are set to zero. Thus, the only non-zero current density is the equivalent magnetic current density $\overrightarrow{M_s}$ along the periphery of the patch. This is shown in Figure 1.3(b). The presence of the ground plane can be taken into account by the image theory, which will double the equivalent current density of 1.2. Therefore, the radiation from the patch can be described to four ribbons of magnetic current (around the periphery) radiating in free space as shown in Figure 1.3(c).

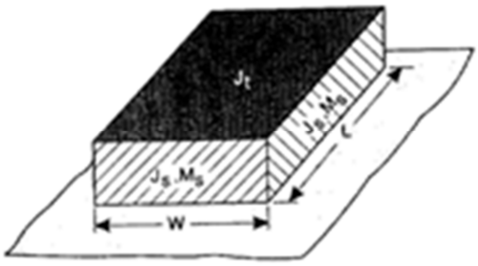

(a)

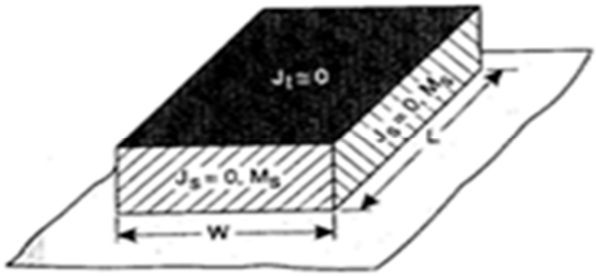

(b)

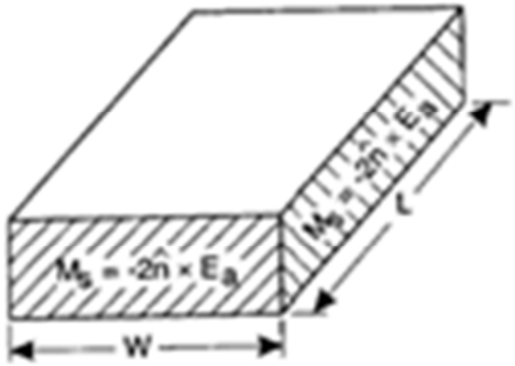

(c)

Figure 1.3. Equivalent current densities on a rectangular microstrip patch (a) J_s and M_s with ground plane, (b) $J_s = 0$, M_s with ground plane and (c) M_s with no ground plane[3]

The new current density is given by

$$\overrightarrow{M_s} = -2\hat{n} \times \overrightarrow{E_a} \tag{1.3}$$

The equivalent magnetic current densities in the slots are shown in Figure 1.4. Using the equivalence principle, each slot radiates the same field as a magnetic dipole with current density $\overrightarrow{M_s}$.

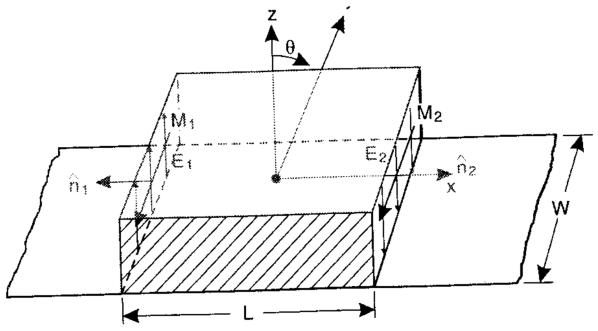

(a)

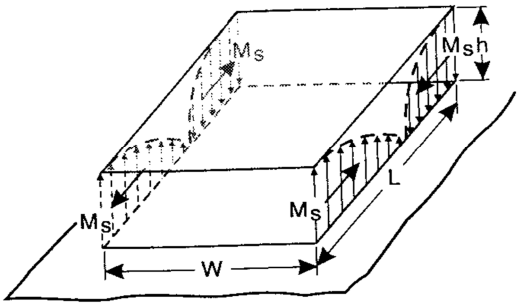

(b)

Figure 1.4. Rectangular microstrip patch with magnetic current density distribution on the radiating slots [3]

The radiation produced by the slots laid out along the x-axis is almost zero because of equal and opposite current distributions on the slots. However, the slots along the y-axis form a two-element array with the current densities of the same magnitude and phase and are separated by length of the patch (L). Therefore, radiation from the patch can be described in terms of two vertical slots.

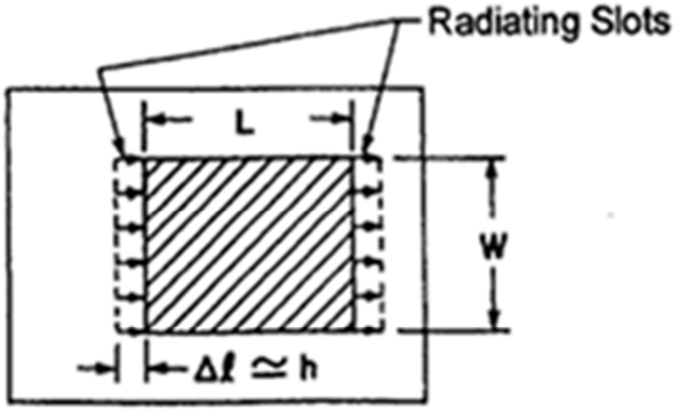

Figure 1.5. Rectangular MPA with equivalent horizontal radiating slots [3]

Vertical slots in the inhomogeneous dielectric of the MPA are difficult to analyse. Therefore, the vertical slots are replaced by two equivalent planar slots as shown in the Figure 1.5.

1.2.2. Methods of analysis of MPAs

Analysis of antenna is important for several reasons:

- It can be used to predict the radiation characteristics such as radiation pattern, gain and polarization as well as near field characteristics such as input impedance, impedance bandwidth, mutual coupling and antenna efficiency.
- The analysis can be used to ascertain the advantages as well as limitations of the antenna by carrying out parametric studies.
- Analysis can provide an understanding of the operating principles that could be useful for a new design, for modifications to an existing design and for the development of new antenna configurations.

Many techniques have been proposed and used to determine MPA characteristics and these include the transmission line model, cavity model and multiport network model. Transmission line model is amongst the most intuitively appealing models that have been proposed for a MPA. This model presents the MPA by two slots, each having width W and height h with separation by a transmission line of length L. The microstrip is substantially a nonhomogeneous line having two dielectrics, usually the air and the substrate.

As depicted in Figure 1.6, the electric field lines reside mostly in the substrate while some lines in air. Consequently, this transmission line cannot guide pure transverse electric-magnetic (TEM) mode of transmission because of the different phase velocities in the air and the substrate. Rather, the dominant mode of propagation would be the quasi-TEM mode. Therefore, in order to account for fringing and the propagation of wave in the line, an effective dielectric constant (ε_{reff}) must be attained.

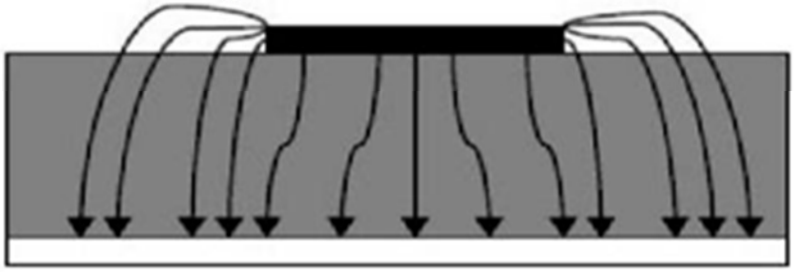

Figure 1.6 Electric field lines in MPA [2]

The value of ε_{reff} is somewhat less as compared to that of ε_r because the fringing fields existing around the patch periphery are not restricted in the dielectric substrate but spread in the air [2] as illustrated in Figure 1.6.

$$\epsilon_{reff} = \frac{\epsilon_r+1}{2} + \frac{\epsilon_r-1}{2}\left[1 + 12\frac{h}{W}\right]^{-1/2} \quad (1.4)$$

where,

ε_{reff} = Effective dielectric constant

ε_r = Dielectric constant of substrate

h = Thickness of dielectric substrate

W = Patch width

Consider Figure 1.7, which represents a rectangular MPA with length *L*, width *W,* on a substrate of thickness *h*. The co-ordinate axis is selected in such a way that the length of patch is along the *x* direction, width of patch is along the *y* direction and the thickness of the patch is along the *z* direction.

.

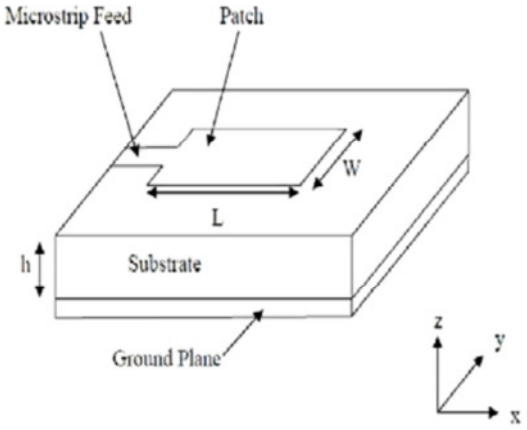

Figure 1.7. MPA [2]

In the Figure 1.8, the MPA is presented by two slots which are open circuit at both the ends and separated by a transmission line of length L. The voltage is maximum and current is minimum along the width of the patch due to the open ends. The fields existing at the edges can be resolved into tangential and normal components with respect to the ground plane.

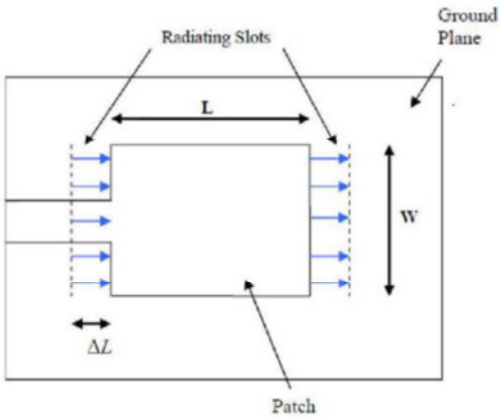

Figure 1.8 Top view of the antenna [2]

It is seen from Figure 1.9 that the normal components of the electric field at the two edges along the width are in opposite directions and thus out of phase since the patch is λ/2 long and hence they nullify each other in the broadside direction. The tangential components, are in phase, which means that these fields combine to yield maximum radiated field normal to the structure surface. Hence, the edges along the width can be presented by two radiating slots, which are separated by length of λ/2, excited in phase and radiating in the half space above the ground plane. The fringing fields existing along the width can be modelled as radiating slots and electrically the patch of the MPA appears enlarged than its physical dimensions [2]. The dimensions of the patch have now been extended by a distance ΔL on each end along its length.

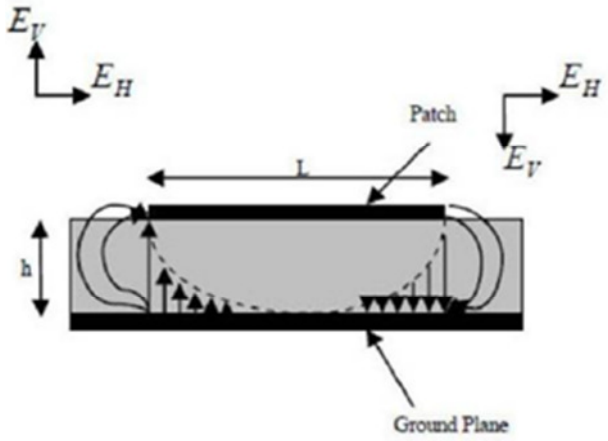

Figure 1.9. Side view of Antenna [2]

$$\frac{\Delta L}{h} = 0.412 \frac{(\epsilon_{reff}+0.3)\,(\frac{W}{h}+0.264)}{(\epsilon_{reff}-0.258)(\frac{W}{h}+0.8)} \tag{1.5}$$

The effective length of the patch L_{eff} now becomes:

$$L_{eff} = L + 2\Delta L \tag{1.6}$$

The frequency at which the MPA resonates is given by

$$f_r = \frac{1}{2L_{eff}\sqrt{\epsilon_{reff}}\sqrt{\mu_0\epsilon_0}} \tag{1.7}$$

The width and length of the patch is given by

$$W = \frac{1}{2f_r\sqrt{\mu_0\,\epsilon_0}}\sqrt{\frac{2}{\epsilon_r+1}} = \frac{\upsilon_0}{2f_r}\sqrt{\frac{2}{\epsilon_r+1}} \tag{1.8}$$

$$L = \frac{1}{2f_r\sqrt{\epsilon_{reff}}\sqrt{\mu_0 \epsilon_0}} - 2\Delta L \quad (1.9)$$

Finally, the length and width of ground is given by

$$L_g = 6h+L \quad (1.10)$$

$$W_g = 6h+W \quad (1.11)$$

where,

h= Substrate thickness

L = Length of patch

W= Width of patch

L_{eff} = Effective length

C= Speed of light

ϵ_r= Relative permittivity

ϵ_{reff}= Effective permittivity

1.2.3. Feeding techniques for MPAs

The prominent feed structures include coaxial feed, microstrip feed, proximity-coupled microstrip feed, aperture-coupled microstrip feed and coplanar waveguide feed.Selection of the feeding technique is governed by a no. of factors.

- The most important consideration is the efficient transfer of power between the radiating structure and feed structure, that is, impedance matching between the two.
- The undesired radiation may increase the sidelobe level and the cross-polar amplitude of the radiation pattern. Minimization of spurious radiation and its effect on the radiation pattern is one of the important factors for the evaluation of feed.

- **Coaxial feed/ Probe Coupling:** One of the fundamental mechanisms for the transmission of microwave power is the coupling of power through a probe. The coaxial connector is attached at the back side of the printed circuit board and the centre conductor (which is coaxial) after passing through the substrate is soldered to

the metallization of the patch. The location of the feed point is determined for the given mode in order to achieve the best impedance match.

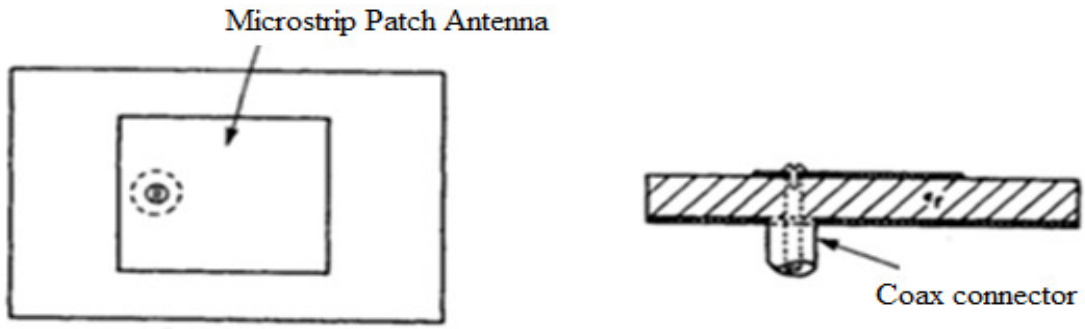

Figure 1.10. Coaxial probe feeding of a MPA (a) Top View and (b) Side View [3]

Coaxial feed has the advantage of simplicity of design since it allows the positioning of the feed point in order to adjust the input impedance level. But it has several limitations. First, coaxial feeding of an array requires a large number of solder joints, which makes fabrication difficult and compromises reliability. Second, for increased bandwidth of a patch antenna, a thicker substrate is used and therefore requires longer probe. This gives rise to an increase in spurious radiation from the probe, increased surface wave power and increased feed inductance.

- **Microstrip line feed:** This type of feed technique employs a conducting strip that is directly connected to the edge of the microstrip patch as shown in Figure 1.11. The conducting strip is smaller in width in comparison to the patch. This feed arrangement has the advantage that the feed can be etched over the substrate thereby providing a planar structure.

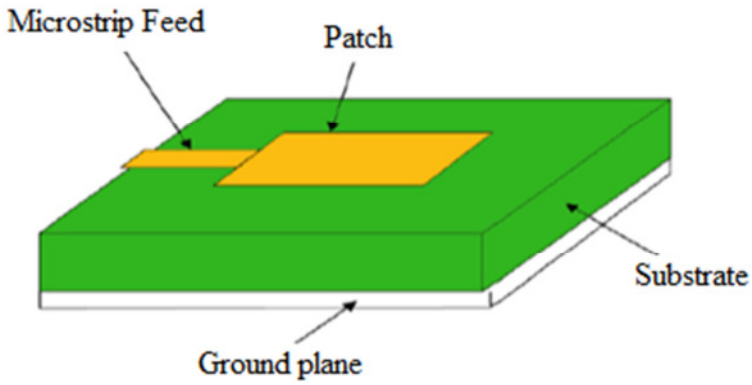

Figure 1.11. Microstrip line feed [4]

This feeding scheme is easy, since it imparts ease of fabrication and at the same time the simplicity in modelling and impedance matching. However, increase in the thickness of the dielectric substrate increases the surface waves and spurious feed radiation, which lowers the antenna bandwidth. The feed radiation also causes cross polarized radiation which is undesirable.

- **Proximity-coupled microstrip feed:** This feeding technique uses two-layerr substrate with microstrip line on the lower layer and patch antenna on the upper layer. The feed line terminates in the open and underneath the patch. Fabrication of this feed is slightly more difficult because of the requirement of accurate alignment between the patch and the feed line.
- **Aperture-coupled microstrip feed:** It uses two substrates separated by a common ground plane. A microstrip feed line on the lower substrate is electromagnetically coupled to the patch through a slot aperture in the common ground plane.
- **Coplanar Waveguide feed:** In this, the CPW is etched in the ground plane of MPA. The advantage of CPW is that the radiation from feed structure is negligible.

In this thesis work, the coaxial feed and microstrip line feed arrangements have been used. This is because coaxial feeding provides the best impedance matching by allowing the adjustment of the feed point and microstrip feed line can be engraved over the substrate in order to have a simple planer antenna configuration.

1.2.4. Applications of MPAs

The MPAs are famous for their performance and robust design. These antennas find applications in various fields such as in the medical field, satellites, military systems and many more. Because of the low cost of the substrate material and the fabrication, these antennas are flourishing in the commercial aspects as well. MPA has a number of applications, some of which have been discussed as follows:

- **Mobile and satellite communication:** Mobile communication demands small, low profile, low cost antennas. MPA meets all the necessities and is therefore designed for use in mobile communication systems. Satellite communication requires circular polarized radiation patterns which can be realized by employing patch with one or two feed point.
- **Global positioning system applications:** MPAs having high permittivity sintered substrate material for global positioning system (GPS). These antennas are circular polarized, very compact.

- **Radio frequency identification (RFID):** RFID is used in various areas like mobile communication, transportation, logistics, manufacturing, health care etc. RFID system usually makes use of frequencies between 30 Hz and 5.8 GHz [5] depending on applications. Fundamentally an RFID system is a tag or transponder and a transceiver or reader.
- **Radar application:** Radar has been utilized for detecting moving targets such as people and vehicles. The MPAs are an ideal choice for radar. The photolithography based fabrication technology permits the bulk production of these antennas with repeatable performance in addition to lower cost and lesser time frame in comparison to the conventional antennas.
- **Reduced size MPA for bluetooth applications:** In this, the MPA operates in the 2400 to 2484 MHz ISM Band. Although an air substrate is introduced, MPA occupies a small volume of 33.3×6.6×0.8 mm^3 [5].

1.3. Overview of Metamaterials

The advent of micro system technologies and nanotechnologies enabled breakthroughs in many different areas of science and technology, offering functionalities well beyond the natural ones. This allowed structuring of materials for various electromagnetic applications in manners which were previously unimaginable. Amongst certainly the well-known examples of novel electromagnetic structures are photonic crystals and the negative refractive index metamaterials, widely known as "left-handed" materials [6]**.** These materials allowed the extension of the operation of passive and active elements for different microwave applications beyond the limits which previously deemed impossible. An additional achievement was an extreme miniaturization of the components. Metamaterials are therefore defined as the artificial materials engineered to impart properties which may not be easily procurable in nature. These materials generally inherit their properties from structure instead of composition, utilizing the inclusion of slight inhomogeneities to accomplish effective macroscopic behavior. In 1968, the theoretical verification of negative index material and left handed (LH) phenomenon in a medium with negative permittivity (ε) and negative permeability (μ) was postulated and pointed out by Veselago [7]**.** His research showed the exhibition of the phase velocity direction opposite to the Poynting vector of the wave propagation in such a medium; the occurrence of backward wave propagation.

1.3.1. Maxwell's Equations and Left-Handed Metamaterial Properties

Most electromagnetic phenomena can be described by Maxwell's equations, first formulated by James Clerk Maxwell in 1860's. The relations of electric and magnetic field quantities which describe the electromagnetic wave are represented by equations (1.12-1.15) [8]:

$$\nabla \times \bar{E} = -\frac{\partial \bar{B}}{\partial t} - \overline{M_s} \tag{1.12}$$

$$\nabla \times \bar{H} = \overline{J_s} + \frac{\partial \bar{D}}{\partial t} \tag{1.13}$$

$$\nabla \cdot \bar{D} = \rho_e \tag{1.14}$$

$$\nabla \cdot \bar{B} = \rho_m \tag{1.15}$$

All quantities are real values in the functions of space and time. ∇ and $\frac{\partial}{\partial t}$ are the spatial and temporal differentiations, respectively.

E = the electric field vector (V/m),

H = the magnetic field vector (A/m),

D = the displacement of electric flux density vector (C/m^2),

B = the displacement of the magnetic flux density vector (W/m^2),

J = the electric current density vector (A/m^2),

M = the magnetic current density (V/m^2).

ρ_e is the scalar electric charge density (C/m^2),

ρ_m is the scalar magnetic charge density (W/m^2)

In order to fully depict the interaction of the electromagnetic fields, Maxwell's equations have to be extended by the constitutive relations as

$$\bar{D} = \varepsilon \bar{E} \tag{1.16}$$

$$\bar{B} = \mu \bar{H} \tag{1.17}$$

where ε is the dielectric permittivity and μ is the dielectric permeability.

Then, the time dependence is assumed as $e^{+j\omega t.}$ Therefore, the time derivatives in equation (1.12) and (1.13) can be replaced as $j\omega$. Maxwell's equations can be then presented as follows:

$$\nabla \times \bar{E} = -j\omega\mu\bar{H} - \overline{M_s} \tag{1.18}$$

$$\nabla \times \bar{H} = j\omega\varepsilon\bar{E} + \overline{J_s} \tag{1.19}$$

In the case of absence of sources, the equation (1.18) and (1.19) can be expressed without electric and magnetic current densities:

$$\bar{k} \times \bar{E} = \omega\mu\overline{H} \tag{1.20}$$

$$\bar{k} \times \bar{H} = -\omega\varepsilon\bar{E} \quad (1.21)$$

where $\bar{k}$ is the wave vector along the direction of the phase velocity ($\bar{k} = \omega\sqrt{\mu\epsilon}$). Before the study of LHMs, the right hand rule in electromagnetism will be reviewed. When the direction of both normal E and H fields are represented by the thumb and the index finger of the right hand respectively, placed at right angles to each other than the middle finger placed at right angle to both the fingers gives the direction of propagation of the wave. In nature, all electromagnetic waves such as light follow this rule which can be stated in mathematical form as in equation (1.22):

$$\bar{E} \times \bar{H} = \bar{S} \quad (1.22)$$

where $\bar{E}$ is the electric field,

$\bar{H}$ is the magnetic field and H

and $\bar{S}$ represents the Poynting vector and the direction of energy and wave propagation.

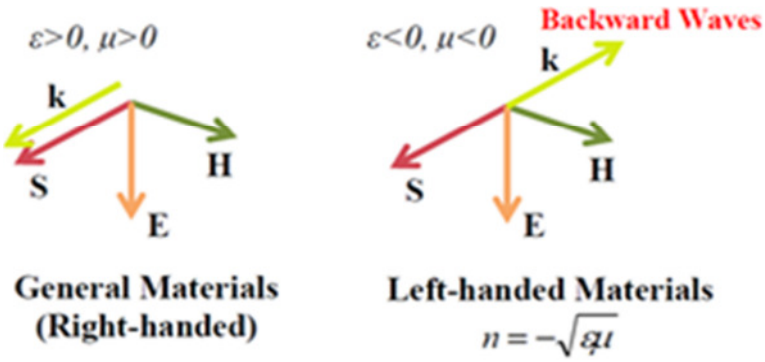

Figure 1.12. Diagrams of electric field, magnetic field, wave vector (E, H, k) and Poynting vector (S) for electromagnetic wave propagation in right-handed and left-handed medium [7-8]

As from the previous Maxwell equations, it can be assumed that in a medium where the permittivity and permeability is negative (LHMs), the phase velocity will be anti-parallel to the direction of wave propagation or energy flow. In another word, the wave has a 'negative phase velocity' in that medium. Even though, the direction of energy flow is always sent from the transmitter to the receiver, the phase moves in the opposite direction, illustrated by the *S* vector which is anti-parallel of *k* vector in Figure 1.12.

1.3.2. Wave radiation in LHMs

As the wave number (k) is anti-parallel with the power flow in LHMs as well as frequency is always a positive quantity, therefore, the phase velocities in RH medium are reverse compared to the LH medium. The phase velocity is defined as:

$$\overline{V_P} = \frac{\omega}{k}\tilde{k} \tag{1.23}$$

where $\tilde{k} = \frac{\bar{k}}{|k|}$

The power flows of LH medium are similar to the RH medium and can be presented as

$$\bar{S} = \bar{E} \times \overline{H^*} \tag{1.24}$$

$$P_0 = \frac{1}{2}\oint \bar{E} \times \bar{H} * \overline{ds} \tag{1.25}$$

where,

S = Poynting vector

P_0 = Power flow

In summarized form, the LH mediums provide the backward wave phenomenon due to the reverse general direction of the phase velocity. The phase velocity is opposite of the oriental direction while the power and group velocity are not affected [8]**.**

To understand a LH system, the equation of refractive index has been defined by the square root of the constitutive parameters which are:

$$\eta = \pm\sqrt{\varepsilon_r}\mu_r \tag{1.26}$$

where η is refractive index and provides negative value in LH medium, ε_r is electric permittivity of material, while μ_r is magnetic permeability of material.

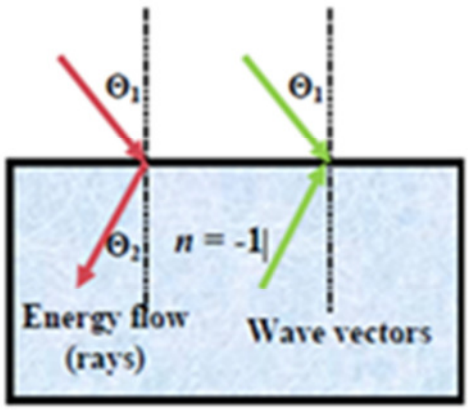

Figure 1.13. Energy flow and wave vector diagram between RH-LH interface

The energy flow vectors are in the same direction, while the wave vectors are in opposite direction (antiparallel) in η = -1 medium, shown in Figure 1.13.

1.3.3. Negative Refraction Phenomenon

In the negative materials, the travelling wave passes from the air through the medium and bends to the same side of the normal as the incident ray. This phenomenon is called negative refraction index, given by the equation (1.27) and as illustrated in Figure 1.14.

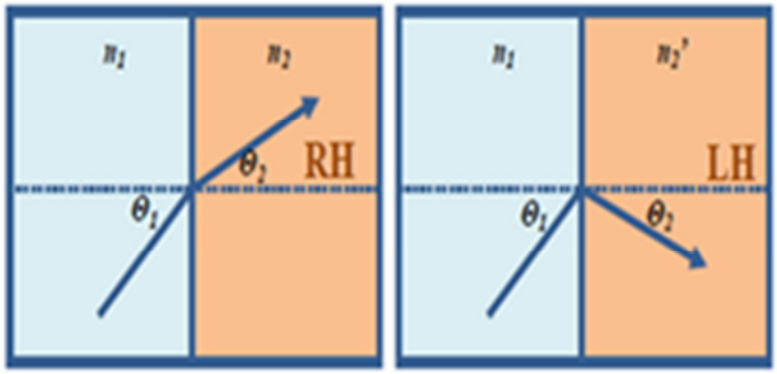

Figure 1.14. The refracted wave in RH and LH medium

The Snell's law supports the wave propagation through LHMs that bended in the wrong way [9]. In Figure 1.14, the refractive index of $n2' = -n2$ and the wave is refracted to the opposite side compared to the ray propagating in Right-Handed (RH) medium. Although the wave bends the opposite direction, the Snell's law is still been satisfied when a negative value of n is substituted and $\theta_2<0$ into the equation,

$$n_1 \sin\theta_1 = n_2 \sin\theta_2 \qquad (1.27)$$

1.3.4. Split Ring Resonators (SRRs):

For decades, and starting in the early 1950s, different ring or ring-like structures with negative permeability were of interest as building blocks for artificial chiral materials in microwave. An SRR as shown in Figure 1.15, is a highly conductive structure in which the capacitance between the two rings balances its inductance [10]. A time-varying magnetic field applied perpendicular to the rings surface induces currents which, in dependence on the resonant properties of the structure, produce a magnetic field that may either oppose or enhance the incident field, thus resulting in positive or negative effective μ. In other words, the operation of an SRR represents an 'over-screened, under-damped' response of material to electromagnetic stimulation.

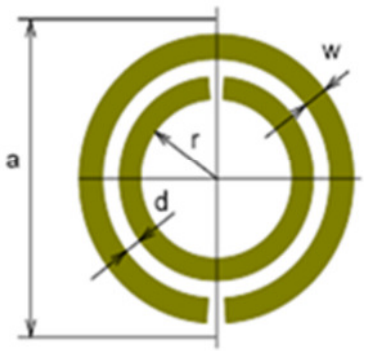

(a)

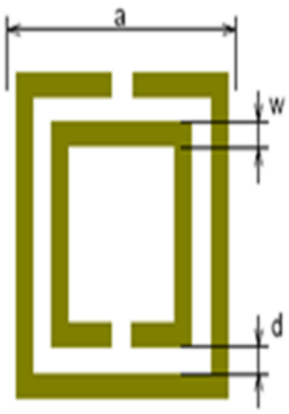

(b)

Figure 1.15. SRR (a) Circular SRR and (b) Rectangular SRR [10]

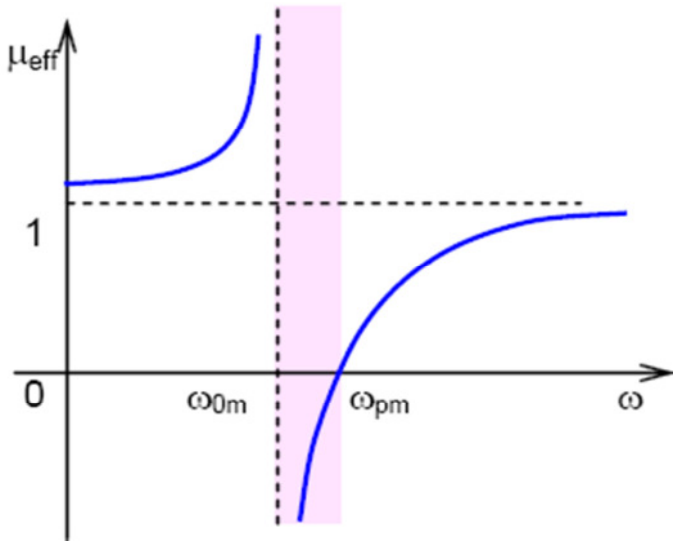

Figure: 1.16. Frequency dependence of effective permittivity for a SRR [10]

The shape of the frequency dependence of ϵ is shown in Figure 1.16. It can be seen that there is a narrow frequency range where the effective permeability is below zero. The resonant frequency is the frequency for which $\mu_{eff} \rightarrow \pm\infty$.

1.3.5. Complementary Split Ring Resonators (CSRRs)

Structures complementary to double split rings were designed and generated on applying the Babinet's principle to the split rings [11]. CSRRs are the structures with apertures in metal surface as shown in Figure 1.17. These CSRRs [11] generate negative ε near the resonance frequency.

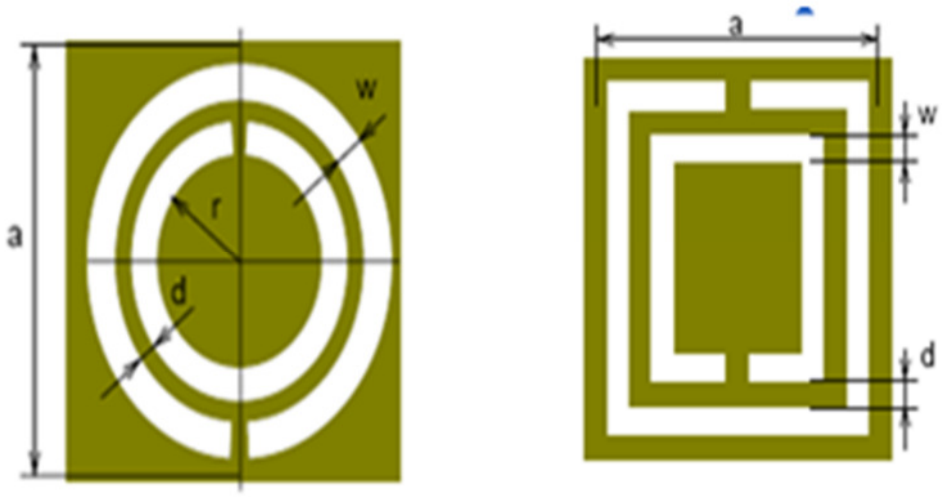

(a) **(b)**

Figure 1.17. Complementary SRR structures (a) Circular and (b) Rectangular [10]

1.3.6. Babinet's Principle:

The design of the complementary split rings resonator, metamaterial with high frequency selectivity and negative dielectric permittivity is based on electromagnetic theory of diffraction and the Babinet principle [11].

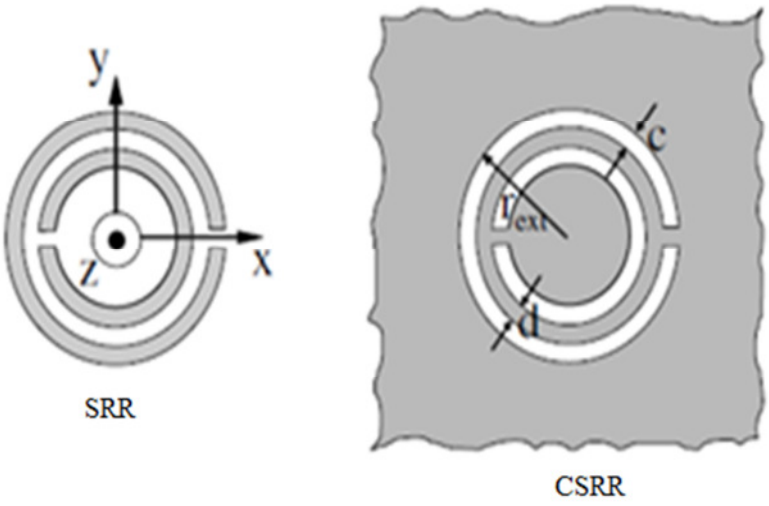

Figure 1.18. Geometries of SRR and CSRR [11]

As a first step in the analysis, the behavior of a perfectly conducting and infinitely thin SRR placed in an external electromagnetic field $\mathbf{E}^0$, $\mathbf{B}^0$ is considered.

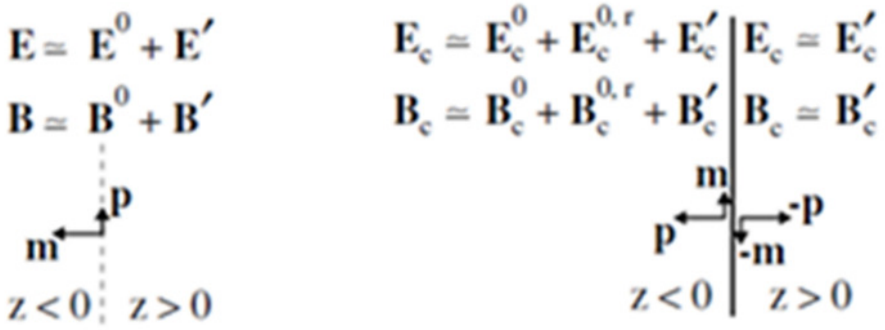

(a) **(b)**

Figure 1.19. Illustration of the behaviour of a (a) SRR and (b) CSRR when illuminated by an external field coming from $z < 0$ [11]

The scattered field $\mathbf{E}^0$, $\mathbf{B}^0$ is approximately given by the field produced by a resonant magnetic dipole [12]

$$\boldsymbol{m} = \alpha_0 \, (\omega_o^2 / \omega^2 - 1)^{-1} B^0 . \hat{z}\hat{z} \tag{1.28}$$

where ω_o is the resonating frequency of the SRR and α_o is a geometrical factor.

Let us now consider the behaviour of the CSRR when it is subjected by an external electromagnetic field $\mathbf{E}_c^0$, $\mathbf{B}_c^0$ from $z < 0$. According to the electromagnetic theory of diffraction [13], the field in the shadowed region ($z > 0$) is the scattered field by the CSRR, $\mathbf{E}_c'$, $\mathbf{B}_c'$. For $z < 0$, the total field is given by [13]

$$\mathbf{E_c} = \mathbf{E}_c^0 + \mathbf{E}_c^{0,r} + \mathbf{E}_c' \; ; \qquad \mathbf{B_c} = \mathbf{B}_c^0 + \mathbf{B}_c^{0,r} + \mathbf{B}_c' \tag{1.29}$$

Where, $\mathbf{E}_c^{0,r}$, $\mathbf{B}_c^{0,r}$ is the reflected field by the metallic screen without the CSRRs etched on it. According to the Babinet principle, if a screen with apertures (the CSRR) is illuminated from $z < 0$ by an incident field $\mathbf{E}_c^0$, $\mathbf{B}_c^0$ and its complementary screen (the SRR) is illuminated by some complementary incident fields $\mathbf{E}^0 = c\mathbf{B}_c^0$ and $\mathbf{B}^0 = -(\frac{1}{c})\mathbf{E}_c^0$ then at the shadowed side ($z > 0$) the total fields must satisfy [13]

$$\mathbf{E_c} - c\mathbf{B} = \mathbf{E}_c^0 \; , c\mathbf{B_c} + \mathbf{E} = \mathbf{B}_c^0 \tag{1.30}$$

Assuming that the SRR scattered field is described by (1.28)**,** it can be easily verified that in order to satisfy (1.30), the fields scattered by the CSRR at $z > 0$, $\mathbf{E}_c'$, $\mathbf{B}_c'$ should be those produced by an electric dipole $p = \left(\frac{1}{c}\right) m$, or

$$p = -(\tfrac{1}{c^2})\alpha_0 \, (\omega_o^2 / \omega^2 - 1)^{-1} . \mathbf{E}_c^0 \; \hat{z}\hat{z} \, .$$

In the nonshadowed region ($z < 0$) the sign of this dipole must change, in order to produce the aforementioned symmetry properties of the scattered fields. Thus, for $z < 0$ we finally obtain

$$\boldsymbol{p} = \alpha_{0,c} \, (\omega_o^2 / \omega^2 - 1)^{-1} . \mathbf{E}_c^0 \; \hat{z}\hat{z} \; ; \; \alpha_{0,c} = (\tfrac{1}{c^2})\alpha_0 \tag{1.31}$$

where c is the velocity of light in vacuum.

The aforementioned results can be directly applied to the design of artificial metasurfaces. In fact, the results for a single CSRR can be extended to a system of many CSRRs with a density of *N* CSRRs per square meter. Since the CSRRs are electrically small [3], the distance between them can be made much smaller than the incident radiation wavelength. Thus we are in the long wavelength limit, and the considered metallic surface can be seen—from the source side—as an electric dipolar sheet of magnitude $\boldsymbol{P}_s = \frac{1}{2}N\boldsymbol{p}$ on top of a flat metallic screen. From the opposite side, a dipolar sheet of the same intensity but of opposite sign is seen. Let us consider the incidence of a plane wave on a CSRR metasurface. Assuming that the angle of incidence and the polarization of this wave allows for the CSRRs excitation, the induced dipolar sheet also produces an electromagnetic wave which interferes with the plane wave reflected at the metallic screen. The effect of this interference can be dramatic near the resonance ω_o . In particular, the CSRRs screen could be potentially tailored in order to destroy the reflected wave. At this frequency all the electromagnetic power will be transmitted through the screen.

1.4. Thesis Outline

The thesis has been sub-divided into seven chapters

In **Chapter 1,** the basics of MPA, an overview of metamaterials and principle of operation of CSRR have been discussed.

In **Chapter 2,** literature survey based on MPA with CSRR has been discussed. In literature survey brief idea of researchers work for size miniaturization, return loss and bandwidth improvement and gain enhancement has taken. Research gaps and thesis objectives have also been defined.

In **Chapter 3**, design and simulation of two coplanar rectangular MPAs with and without slotted CSRR in the ground plane operating around 5 GHz with coaxial feeding technique and their parametric analysis has been discussed and compared.

In **Chapter 4**, design and simulation of a dual band MPA with CSRRs for WLAN applications has been discussed.

In **Chapter 5**, the work done in Chapter 4 has been extended for a multiband MPA with CSRRs. Its simulation and parametric study has been carried out. Finally, the fabrication and testing of antenna is done. Also, the simulated and tested results have been compared

In **Chapter 6**, conclusion of overall thesis and future scope has been discussed.

CHAPTER-2
LITERATURE REVIEW

2.1. Literature Overview

The following research papers that have been performed previously by other researchers have been studied.

V. Rajeshkumar *et al*. (2013) proposed a MPA in which CSRRs are employed in the ground plane. The suggested antenna exhibits dual band characteristics. The simulation results when examined, demonstrated that with the proposed structure, reduction in size of the antenna along with dual band operation can be attained. Also, the variation in resonant frequency with the change in CSRR length is analysed. A reduction of about 89% in the size of the radiating patch is attained in comparison to conventional MPA [13].

I. B. Issa *et al.* (2013) presented a compact antenna incorporating multi-band square complementary SRR. Because of its compact size, the antenna size can be integrated easily within RF front-end circuits in mobile handsets. The antenna can efficiently cover various frequency bands and wireless communication standards, namely, 2.4GHz (WiFi), 3.5GHz (WiMax), 7.8-9.1GHz (UWB), and 10.9-11.5GHz, and 17.2-17.8GHz frequency bands. Moreover, gain values of the antenna make it appropriate for both indoor and outdoor wireless communications [14].

M. M. Bait-Suwailam *et al.* (2013) suggested a novel design for miniaturization of MPAs with a slotted CSRR inclusion known as SCSRR. The design also proposed mutual coupling reduction between MPAs. Numerical studies were carried out using CST Microwave Studio. A size reduction of almost 10% has been achieved for MPA when SCSRRs are etched in ground plane [15].

S. C. Basaran *et al.* (2013) suggested a complementary split-ring resonator based monopole antenna using three-stage microstrip line feeding. The resulting antenna is electrically small and finds application in 3.5 GHz WiMAX and 2.4/5.2 GHz WLAN bands. The antenna exhibits an improved impedance bandwidth performance of 13, 17 and 16% at the three respective bands [16].

M. U. Vakani *et al.* (2012) focused on developing miniaturized antenna, having capability to resonate over more than one band. Initially they analysed square patch antenna with its S11 Parameters, and gain characteristics. Then structure based on SRR

was analyzed with similar antenna characteristics. LC resonance behavior of SRR gives it capability to resonate at sub wavelength sizes. It was observed that SRR based antenna is small and flexible to designers as antenna could be made to resonate at desired frequency just by scaling its dimensions. There are various antenna miniaturization techniques for MPAs like use of high dielectric constant materials, the introduction of slots on the resonant patch etc. All these technique can be applied for miniaturization but they provide limited size reduction, use of high dielectric constant degrades the antenna performance because of surface waves.The work demonstrated that simple SRR structure gave 85% footprint size reduction compared to conventional square patch antenna, with bandwidth 5% and gain 1.6dB, structure with strip inside SRR gives 94% size reduction with bandwidth 6% and gain 1.4dB, while structure with multiple concentric rings gave more bands and 92% size reduction, with bandwidth 5.4% and 4.1% and gain 1.7dB. Hence, small sized dual or multi band antenna is possible with SRR [17].

S. C. Basaran (2012) suggested a dual wideband split-ring antenna for WLAN applications. The proposed antenna is fed by CPW and has a compact size. The antenna can cover almost all WLAN operation bandwidths (2.4-2.485 GHz, 5.15-5.35 GHz, and 5.725-5.825 GHz). Also, the proposed antenna exhibits almost omni-directional radiation patterns with predicted gains of 5 dBi over the bands of interest. Hence, it can fully meet the requirements of indoor wireless applications [18].

Y. Dong *et al.* (2012) investigated compact patch antennas with complementary split-ring resonators (CSRRs) and reactive impedance surface (RIS) loading. The incorporated CSRR on the patch acts as a shunt *LC* resonator in order to provide a low resonance frequency. Both the CSRR and the RIS were able to reduce the size of the antenna. Multi-band operation with varied polarization states can be attained by employing different configurations of the CSRRs. The CSRR was embedded on the top surface as a high-quality factor resonator, excited by the orthogonal electric field, which could couple the field to the antenna patch and made it to radiate [19].

W. Cao *et al.* (2011) presented a compact patch antenna having low-cost with ability of steering the beam. The ground structure with CSRR-loading results in a wide-scale steering range and can very efficiently lower the cost of a phased-array system in order to meet the demands of the wireless communications. The refractive index of the loading part affects the beam direction [20].

X. Cheng *et al.* (2011) designed and fabricated a CSRR loading based patch antenna on a substrate that is flexible and can be folded in a cylindrical shape resulting in a nonplanar

CSRR loaded patch, featuring compact size, EMI shielding, and quasi-omnidirectional radiation pattern for a wireless endoscope. Also, the antenna took the advantage of the slot inherent to the folded patch and negates the necessity of any external matching circuit. All the endoscope circuits could be wrapped around by the antenna [21].

Ó. Quevedo-Teruel *et al.* (2011) presented and studied a strongly miniaturized MPA based on SRRs . In virtue of its two concentric rings, this antenna provided two simultaneous bands of operation. A parametric study of the operation frequency has been performed, showing how it is influenced by the dimensions of the rings. Results have shown that the total size of the rings and the permittivity of the dielectric substrate have a significant effect on these resonances. In this paper, SSRs have been used with traditional antennas for obtaining new resonances, or to modify the radiation pattern or the usual operation frequency. The antenna is dual-band and highly compact, and consequently can be suitable for applications where there are size constraints. Compact antennas with dual band performance have been explored in the literature. Most of the compact antennas use substrates with high permittivities. This paper proposed an antenna whose size is compact even with low permittivity materials. Some new patch antennas that use SSRs for defining new operation bands (at lower frequencies) have also been presented [22].

N. Ortiz *et al.* (2011) suggested that on etching a complementary rectangular SRR on the patch of a conventional rectangular patch antenna, a vertical polarized dual band rectangular patch antenna is achieved. The CSRR etching at some positions of the patch results in the reduction of both patch antenna resonances, resulting in miniaturization of the dual band antennas. In contrast to the resonating frequency of a rectangular slot, the frequency at which the CSRR resonates becomes much lower for the same physical size. The suggested design therefore comes as an alternative solution to the dual band antenna designs existing now-a-days [23].

S. S. Pattnaik *et al.* (2010) proposed a planar metamaterial MSRR loaded electrically small MPA of high gain and efficiency. The metamaterial characteristics of MSRR unit cell and the results of unloaded and loaded electrically small rectangular MPA are presented and analysed. This type of antenna will find its applications in wireless and mobile communication systems, wearable devices and radiometer systems [24].

L. Ke *et al.* (2010) proposed a circularly polarized MPA,design based on the single CSRR. The CSRR structure is composed of one concentric metallic slot rings, interrupted by a small gap. In this paper, a single-feed circularly polarized MPA using the CSRR etching on the radiation patch was analyzed and fabricated. The major advantage of this

type single-feed, circularly polarized MPAs is their low profile and relatively simple structures, which does not require an external polarizer and can conveniently be integrated into the equipments requiring compact dimension, such as handset. It can, therefore, be realized more compactly by using less board space than dual-feed circularly polarized MPAs can be [25].

M. M. Bait-Suwailam *et al.* (2010) introduced a structure based on CSRRs to reduce the mutual coupling between two coplanar MPAs that radiate in the same frequency band. The new unit cell consists of two complementary SRR inclusions connected by an additional slot. Using the new structure, it was possible to achieve a 10-dB reduction in the mutual coupling between two patch antennas with a separation of only 1/4 free-space wavelength between them. The proposed structures being broadband can be used to minimize coupling and co-channel interference in multiband antennas [26].

J. J. Ma *et al.* (2010) designed and fabricated a reduced size MPA. The presence of the negative effective permittivity and permeability produced by the CSRR array etched on the ground plane led to the antenna size reduction. The numerical and measurement results have shown that 35 percent patch size reduction can be achieved between the antenna with CSRR as well as comparison the one without it [27].

C. J. Sanchez-Fernandez *et al.* (2010) proposed an innovative dual band MPA for Implantable Medical Devices (IMD). Implantable medical devices such as cardiac pacemakers and glucometers, are used clinically for administering therapy and for physiological monitoring. By using antennas, implantable devices can establish a communications link to external devices. As main requirements, these antennas should have a small size and a reasonable radiation efficiency. Another important aspect is the effect of the body on the characteristics of the antenna, which makes it mandatory to take into account the dielectric properties of the different tissues inside the human body for a proper and realistic antenna simulation and design. Particularly, antenna must work at the two bands commonly employed in these applications: MICS (402-405 MHz) and ISM (2.4-2.48 GHz). The feeding line and radiating layer were located at different levels in the proposed structure. The radiating element of the antenna which was a SRR, was coupled to a Spiral. In order to achieve size reduction, both the elements were short-circuited to the ground plane. Moreover, the effects of geometry of the human body and properties of dielectric were studied [28].

N. Ortiz *et al.* (2009) presented a simple dual band patch rectangular antenna design. The dual band antenna was attained when a complementary rectangular SRR is etched over

the patch of a conventional rectangular patch antenna, and also a miniaturization of the conventional antenna is attained. Because of the quasi-static resonance property inherent in the complementary SRRs, the dual band antenna design was made possible [29].

S. R. BhadraChoudhuri *et al.* (2009) realized CSRR array on the ground plane along the length of a rectangular MPA that improved the gain by providing better match at the desired resonant frequency. Dual band operation was also observed when the array of CSRR designed at double the RMSA resonant frequency was inserted half way underneath the patch. The CSRR are favorable for microstrip applications as it responds to axial electric field. The work demonstrated that there was a sharp improvement in return loss when the CSRR were etched out in the ground plane [30].

H. Zhang *et al.* (2008) studied the design of MPA with circular polarization based on CSRR. For a good circular polarization radiation, in order to excite the square MPA, the non-resonant property of CSRR was utilised as an asymmetric perturbation. Circular polarization (CP) MPA technology has spawned wide applications of military and the mobile wireless communications because they are not only able to reduce the multi-path effect but also allow more flexible orientation of the transmitter and receiver antennas. The CP radiation was achieved by simply embedding a CSRR on the square patch antenna. The splits on the ring slots were taken asymmetric to the surface current paths of the original patch antenna and thus its fundamental resonant mode was split into two resonant modes which was tuned for a good circular polarization (CP) radiation [31].

R. KarimzadehBaeel *et al.* (2007) presented a compact MPA with size reduction via the use of CSRRs. When CSRRs were placed, the shift in the resonant frequency to a lower value was observed which suggested a reduction in patch size. The size of patch antenna reduced about 25% without increasing the substrate dimension. MPA loaded with CSRRs was modeled by means of a lumped element circuit model in this paper [32].

A. U. Limaye *et al.* (2007) focussed on using CSRR as LHMs for size reduction of MPAs. The frequency response for each antenna with and without CSRR and a shift in resonant frequency has been calculated. It has been shown that the frequency shifted to a lower value for the same size of the patch when it has CSRRs in the ground plane. The CSRRs being slots in the ground plane may behave as radiators and therefore the back lobe radiation has been addressed and it has been concluded that the back lobe radiation could be reduced significantly if the CSRR used under the patch has a stop-band corresponding to the desired resonant frequency of the antenna [33].

Y. Lee *et al.* (2007) investigated a MPA on a dielectric substrate with CSRRs employed in the ground plane. One of popular approaches for miniaturization of MPAs is to use a high permittivity dielectric substrate in order to decrease the guided wavelength, and hence the overall antenna size. However, it has drawbacks resulting in the tendency for more of the energy delivered to the antenna to be trapped in substrates with high permittivities, which eventually decreases the impedance bandwidth. This paper proposed a new design approach to the realization of compact antennas with improved bandwidth using a ground plane loaded with CSRRs. The resonant frequency, impedance, bandwidth, and radiation characteristics were examined. The comparison of the impedance bandwidth between the MPA on a conventional high permittivity substrate and with the CSRR substrate was presented. The antenna so fabricated achieved a 69% reduction in the resonant frequency as well as 67% improvement in the bandwidth compared to the conventional antenna [34].

J. D. Baena *et al.* (2005) analysed split-ring resonators and their dual counterparts complementary split-ring resonators which are integrated to planar transmission lines. The electromagnetic behavior of these elements has been investigated. The equivalent-circuit models for the isolated and coupled SRRs/CSRRs have been discussed. From which it has been concluded that in the long wavelength limit, the stopbands/passbands are the outcome of the presence of negative/positive values for the effective ϵ and μ of the line. The stopband/passband characteristics of the proposed transmission line with SRR/CSRR loading have been mathematically analysed [35].

2.2. Thesis Objectives

The following objectives had been designed to carry out the thesis work:

- To design and simulate two coplanar rectangular MPAs with and without slotted CSRR in the ground plane operating around 5 GHz with coaxial feeding technique and their parametric analysis.
- To design and simulate a dual band MPA with CSRRs for WLAN.
- To design and simulate of multiband MPA with CSRRs for wireless applications.
    - Parametric studies on the proposed antenna.
    - Fabrication and testing of the proposed design.
    - To compare the simulated and measured results for the proposed MPA.

2.3. Methodology

- Extensive literature survey has been carried out to study the literature available in the field of dual and multiband MPAs.

- Detailed study of antenna structures.
- The effects on return loss, VSWR, gain and radiation pattern have been analysed.
- In order to carry out simulation of proposed antenna designs, Computer Simulation Technology - Microwave Studio Version 10.0 (CST MWS V10.0) has been used.
- The return loss or S_{11} parameters of the proposed antennas have been measured using Vector Network Analyser.

CHAPTER- 3

RETURN LOSS IMPROVEMENT AND MUTUAL COUPLING REDUCTION IN COPLANAR RMPA WITH CSRR

3.1. Introduction

In this chapter two designs, first one consisting of two coplanar rectangular MPAs without slotted CSRRs and the second one with slotted CSRRs in the ground plane have been presented. The two patch antennas have been placed 1/4 free-space wavelength apart and are excited using coaxial feeding technique. Both patches radiate in the same frequency bands. The parametric analysis of Design 1 (with no CSRR) has been carried out while for the design 2, the effect of CSRR on different parameters such as return loss, bandwidth, mutual coupling and current distribution has been studied. Finally, the comparison of design 1 and design 2 is done.

3.2. Antenna Design 1

The simulated design of the two coplanar MPAs without slotted CSRRs in the ground plane has been shown in Figure 3.1. Design specifications have been discussed in Table 3.1.

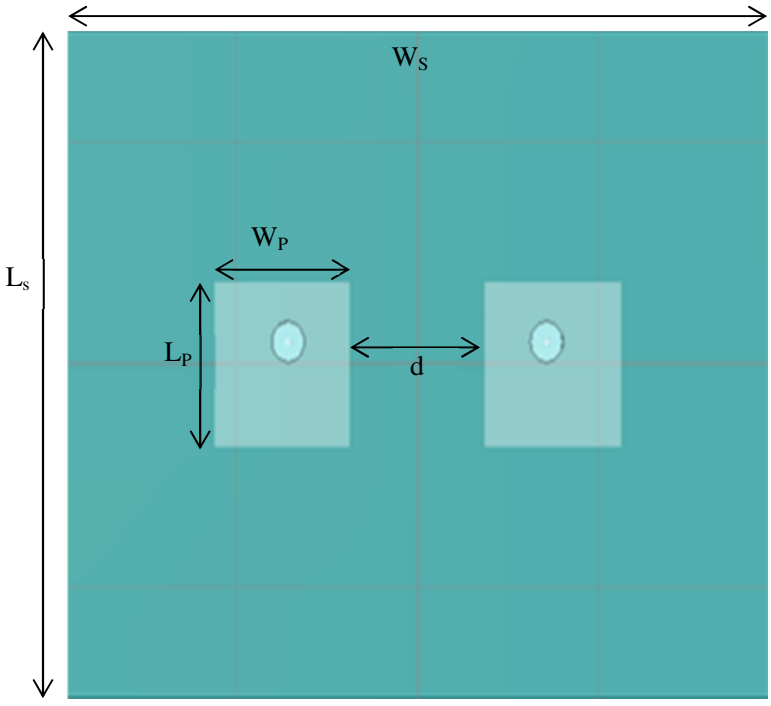

Figure 3.1. Front view of the proposed Design

Table 3.1. Design Specifications of Design 1

Dielectric constant (ϵ_r) of the substrate	3.48
Thickness of the substrate	1.27 mm
Length of the patch(L_p)	15 mm
Width of the patch(W_p)	15 mm
Length of the substrate(L_s)	60 mm
Width of the substrate (W_s)	78 mm
Separation between the two patches(d)	15 mm

3.2.1. Simulated results

- **Return loss:** Return loss is a measure of the difference between the power delivered to the antenna and the power reflected back from the antenna and is generally measured in dB. The smaller the value of return loss, the maximum power is radiated by the antenna. The simulated antenna design resonates at 4.958 GHz and exhibits return loss of -26.0165 as shown in Figure 3.2.

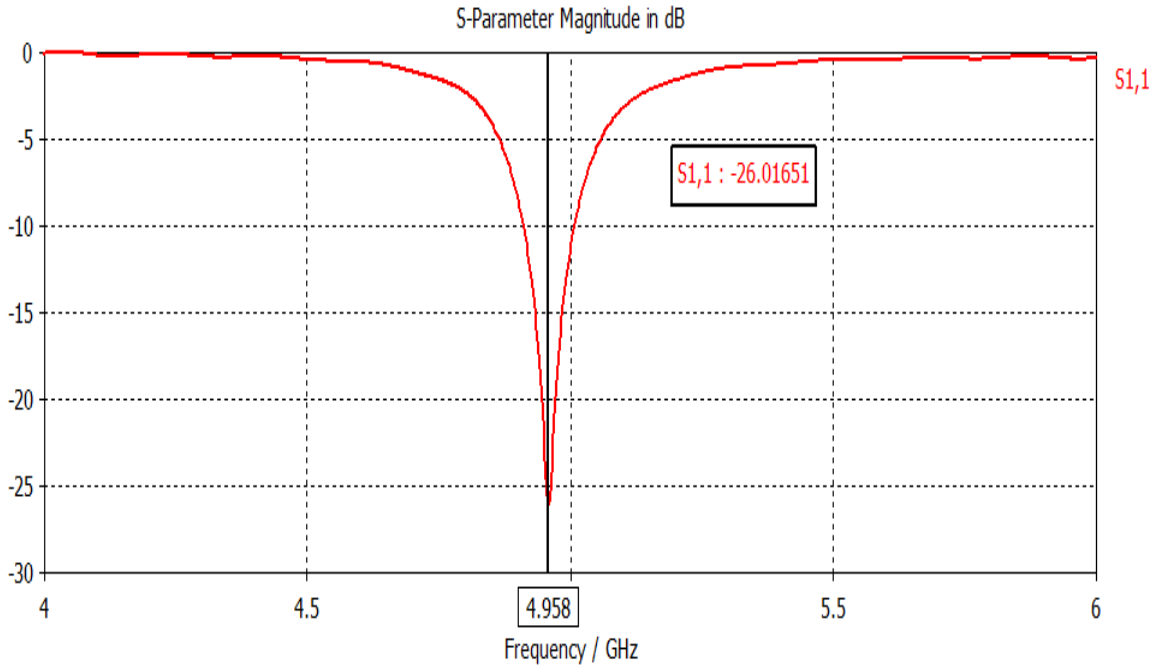

Figure 3.2. Return Loss (S_{11}) Characteristics of Design 1

The bandwidth achieved with this design is 97.5MHz as shown in Figure 3.3.

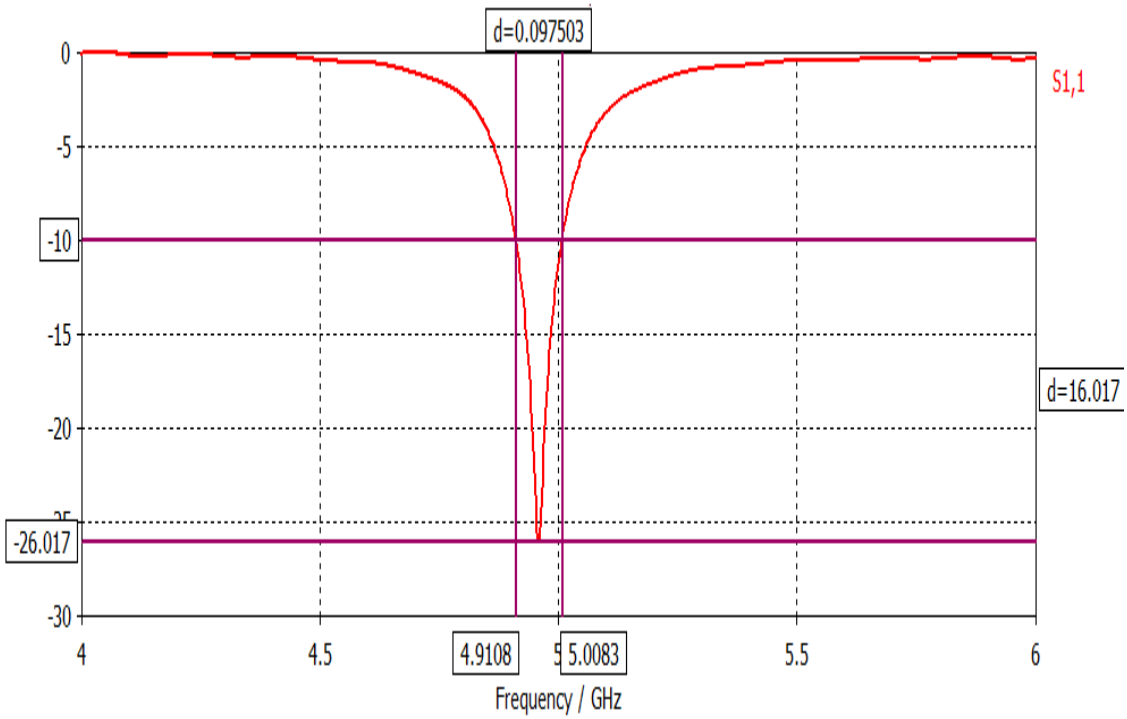

Figure 3.3. Plot for Bandwidth for Design 1

The value of S_{12} parameter, which is a measure of electromagnetic interaction between the two antenna elements (patches), comes out to be -18.621 dB as shown in Figure 3.4.

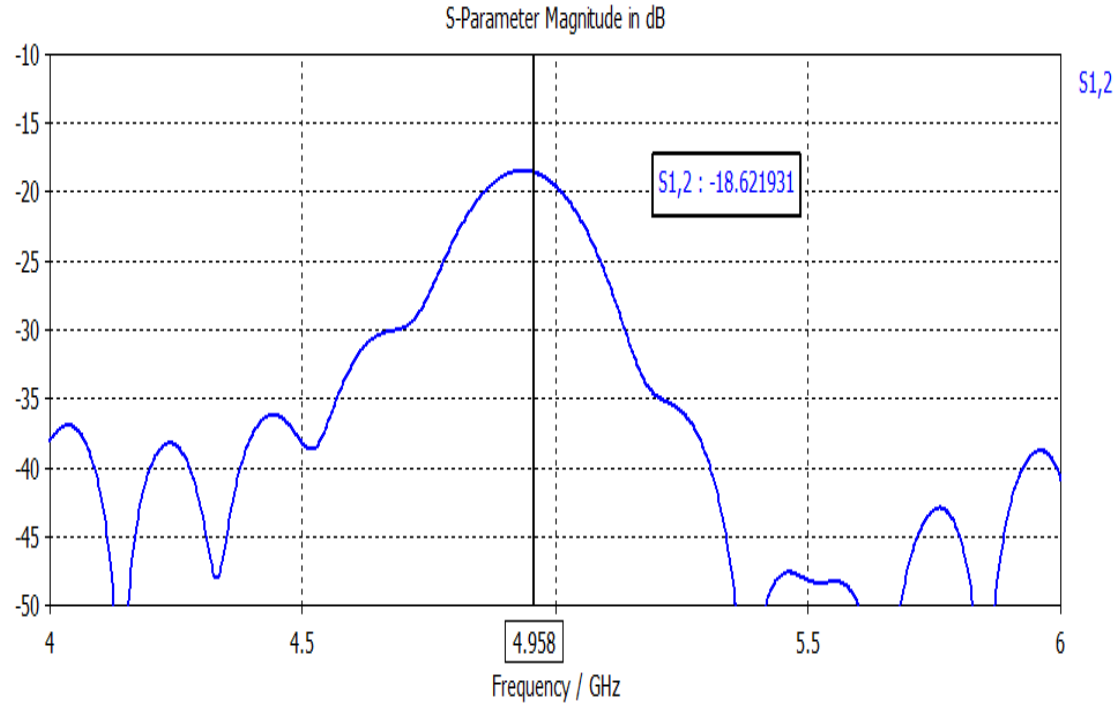

Figure 3.4 Plot for S_{12} parameter for Design 1

- **VSWR:** In order to deliver power to the antenna, the impedance of the antenna must be properly matched to the feedline through which antenna is connected to the transmitter. Reflected waves result if the matching between the two is not proper. The interaction between the reflected waves and the forward waves results in standing waves which are undesirable. Therefore, the ideal value of VSWR should be in between 1 and 2. For this design, the value of VSWR comes out to be 1.105 at port 1 and port 2 and therefore, they are overlapping each other as shown in Figure 3.5.

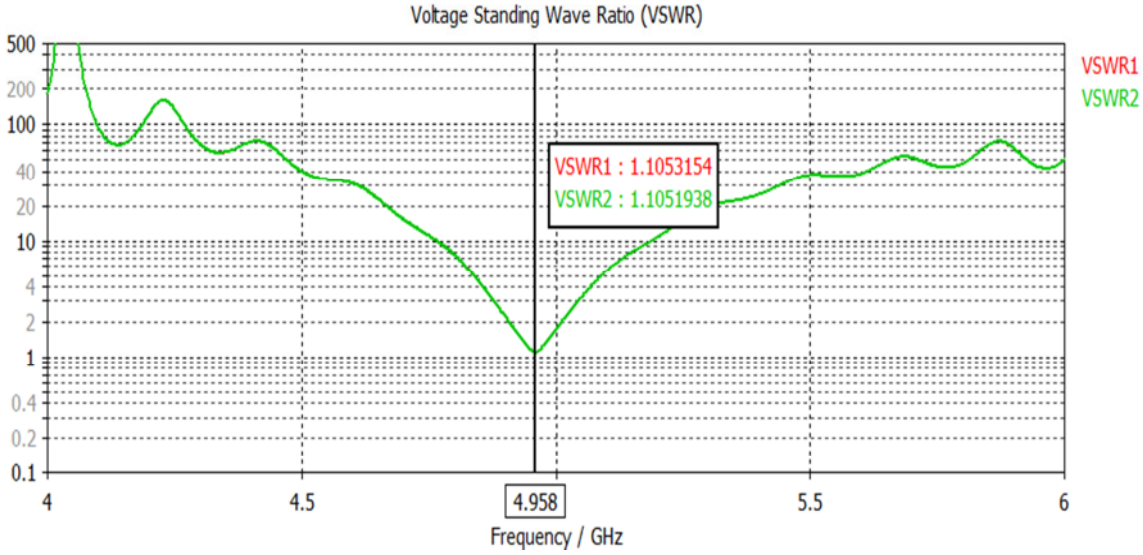

Figure 3.5. Plot for VSWR for Design 1

- **Gain and Directivity:** The 3D plot of gain is shown in Figure 3.6(a) which represents the ratio of power radiated in a particular direction to the power radiated by an isotropic antenna. The value of gain attained is 5.672 dB.

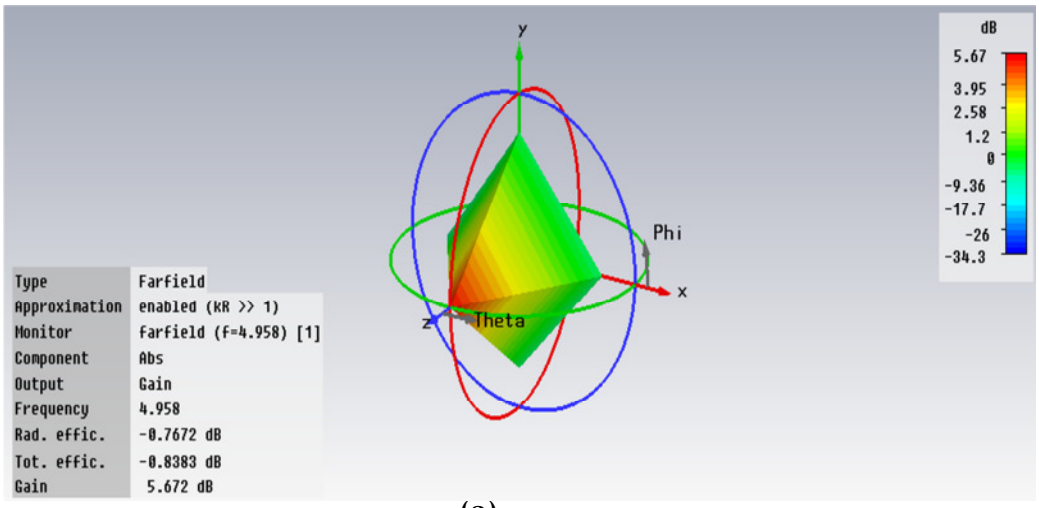

(a)

The 3D plot of directivity is shown in Figure 3.6 (b) which represents the amount of radiation intensity and in this case it is equal to 6.692 dBi. This antenna is directional as the value of directivity is maximum in one particular direction.

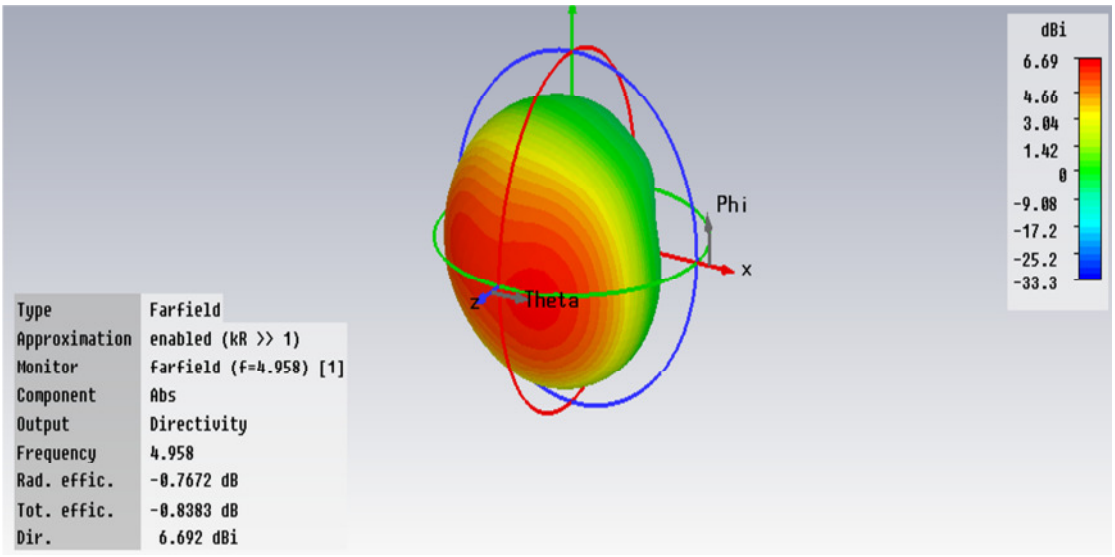

(b)

Figure 3.6. 3D- Plot for (a) Gain and (b) Directivity at 4.958GHz

- **E-field and H-field pattern:** The E-field pattern is shown in Figure 3.7.(a) where the magnitude of main lobe is 12.3 dBV/m. The main lobe is directed along 310.0 deg with an angular width (3 dB) of 100.8 deg. The H-field pattern is shown in Figure 3.7.(b) where the magnitude of main lobe is -31.2 dBA/m. The direction of main lobe is 0.0 deg with half power beamwidth(3 dB) of 83.4 deg.

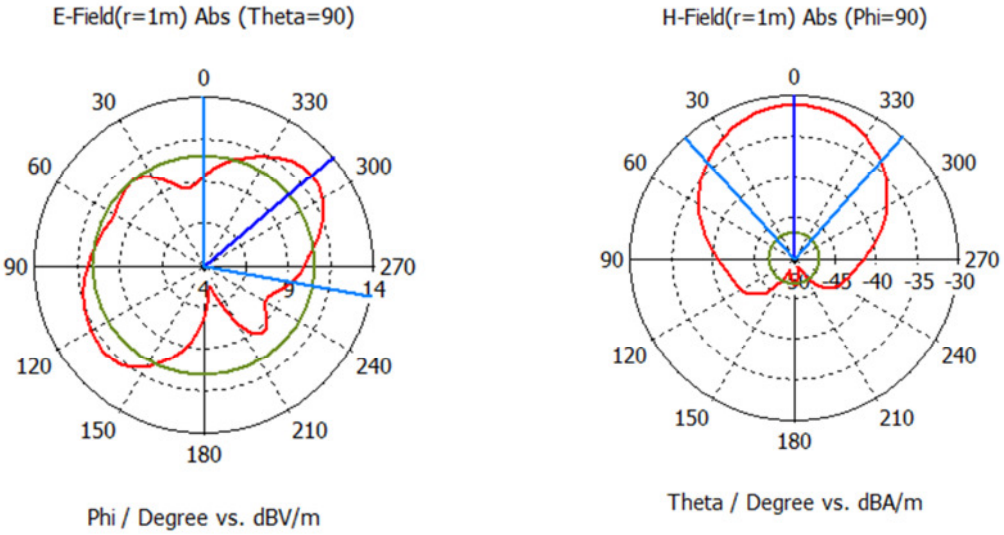

(a) **(b)**

Figure 3.7. Polar plot for the simulated design at 4.958 GHz (a) E-field pattern and (b) H-field pattern

- **Current Distribution:** The surface current distribution when coaxial feeding is provided at port1 has been shown in the Figure 3.8. The current should be maximum at the center of the patch and minimum at edges which are as obtained in this case. Also, it has been observed that there exists mutual coupling between the patches as surface current also exists on the patch 2 as shown.

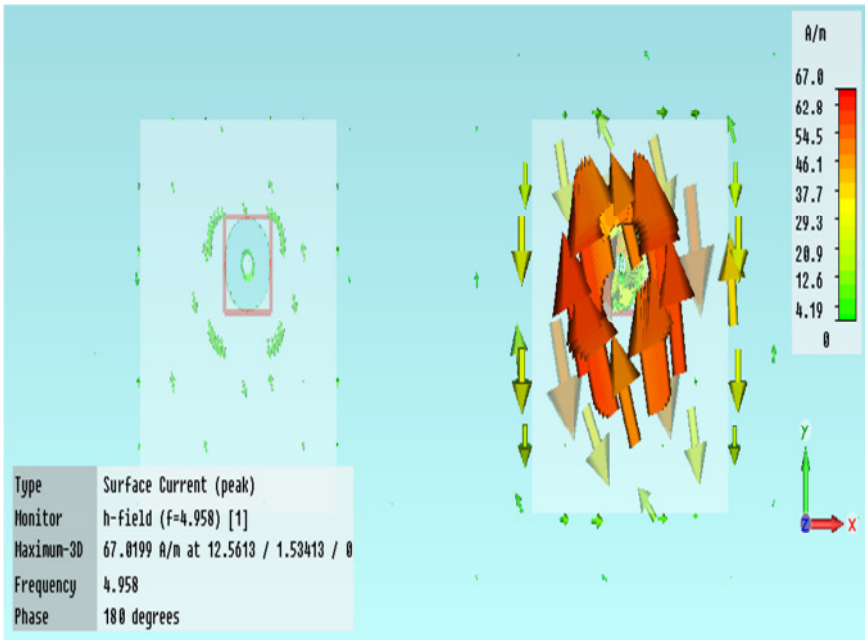

Figure 3.8. Surface current of the Design 1 at 4.958 GHz.

3.3. Antenna Design 2

The simulated design of the two coplanar rectangular MPAs with slotted CSRR has been shown in Figure 3.9. The dimensions of the complementary ring elements have been optimised for required return loss characteristics. The design specifications have been dicussed in Table 3.2.

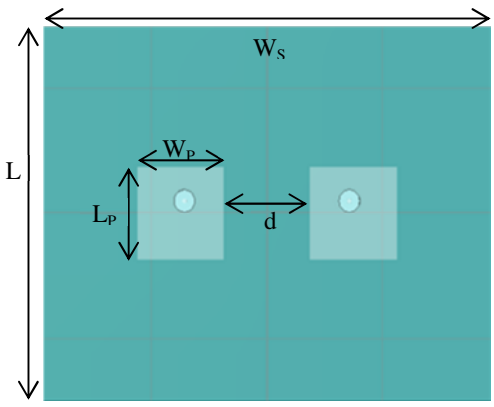

(a)

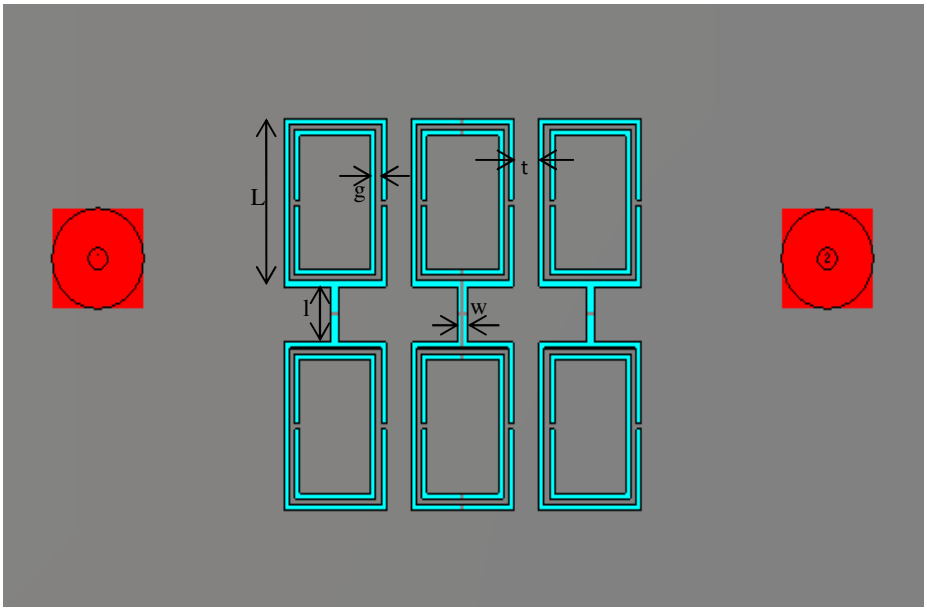

(b)

Figure 3.9 Simulated Design 2 (a) Front View and (b) Back View

Table 3.2. Design Specifications of Design 2

Dielectric constant (ϵ_r) of the substrate	3.48
Thickness of the substrate	1.27 mm
Length of the patch (L_p)	15 mm
Width of the patch (W_p)	15 mm
Length of the substrate (L_s)	60 mm
Width of the substrate (W_s)	78 mm
Separation between the two patches (d)	15 mm
Side Length of slotted CSRR unit cell (L)	4mm
Gap between rings (g)	0.2 mm
Length of slot connecting 2 CSRRs (l)	2 mm
Width of slot connecting 2 CSRRs (w)	0.35 mm
Separation between 2 slotted CSRRs (t)	1 mm

3.3.1. Simulated results:

- **Return Loss:** The simulated antenna design resonates at 4.956 GHz and exhibits return loss of -54.398 dB as shown in Figure 3.10.

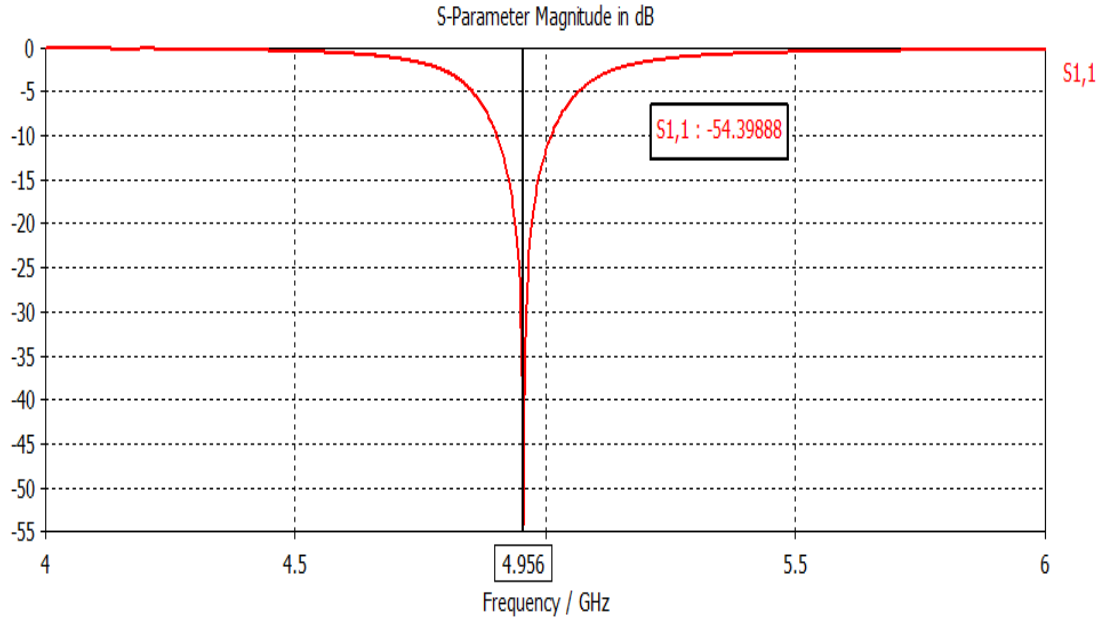

Figure 3.10. Return Loss Characteristics of Design 2 at 4.956 GHz

The bandwidth achieved with this design is 112.28 MHz as shown in Figure 3.11.

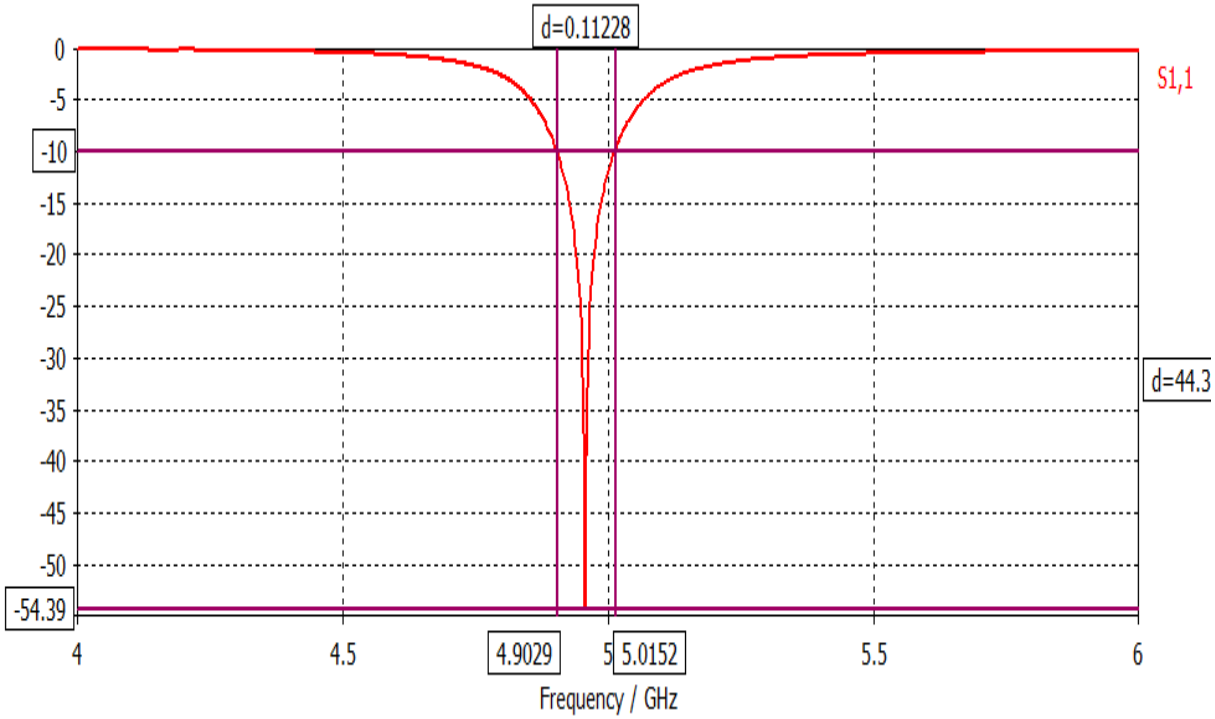

Figure 3.11 Plot for Bandwidth for Design 2.

The value of S_{12} parameter for this design is -20.0566 dB as shown in Figure 3.12.

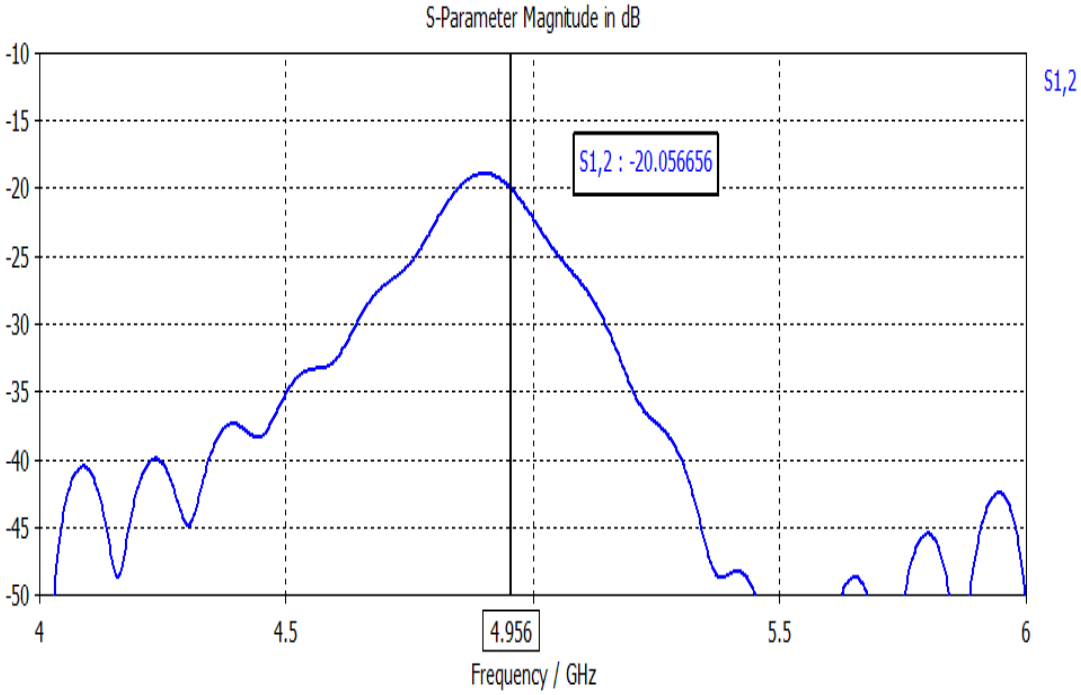

Figure 3.12. Plot for S_{12} parameter for Design 2

- **VSWR:** The value of VSWR at 4.956 GHz comes out to be 1.0038 as shown in Figure 3.13 which is below 2 as desired.

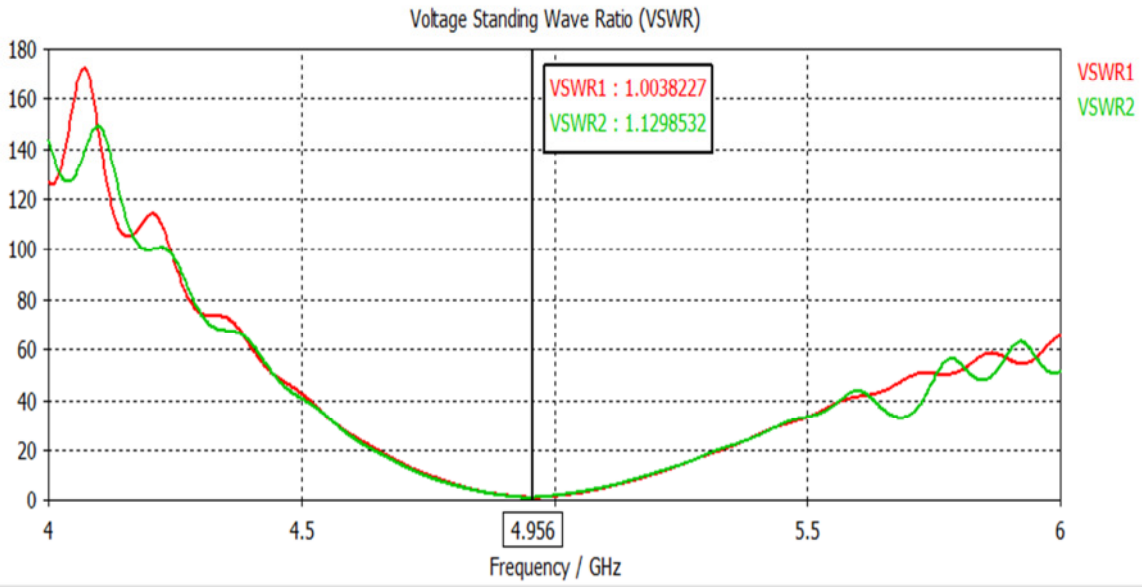

Figure 3.13. Plot for VSWR for Design 2 at 4.956 GHz

- **Gain and Directivity:** The 3D plot of gain is shown in Figure 3.14 (a). The value of gain attained is 5.672 dB.

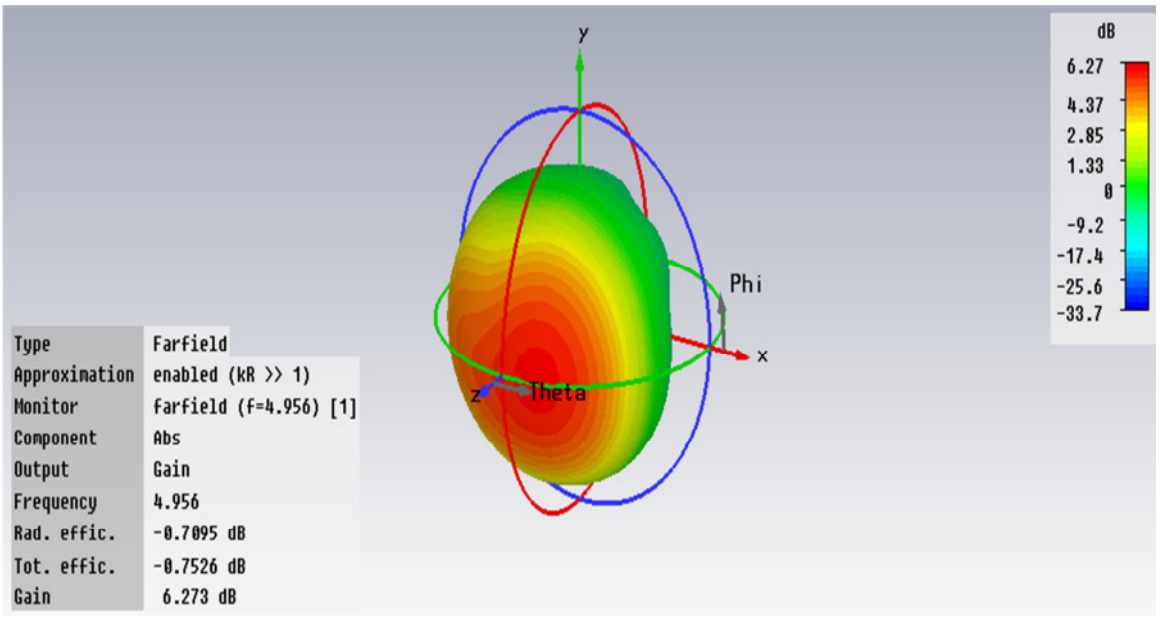

(a)

The 3D plot of directivity is shown in Figure 3.14(b). From the plot, the value of the directivity comes out to be 6.982 dBi.

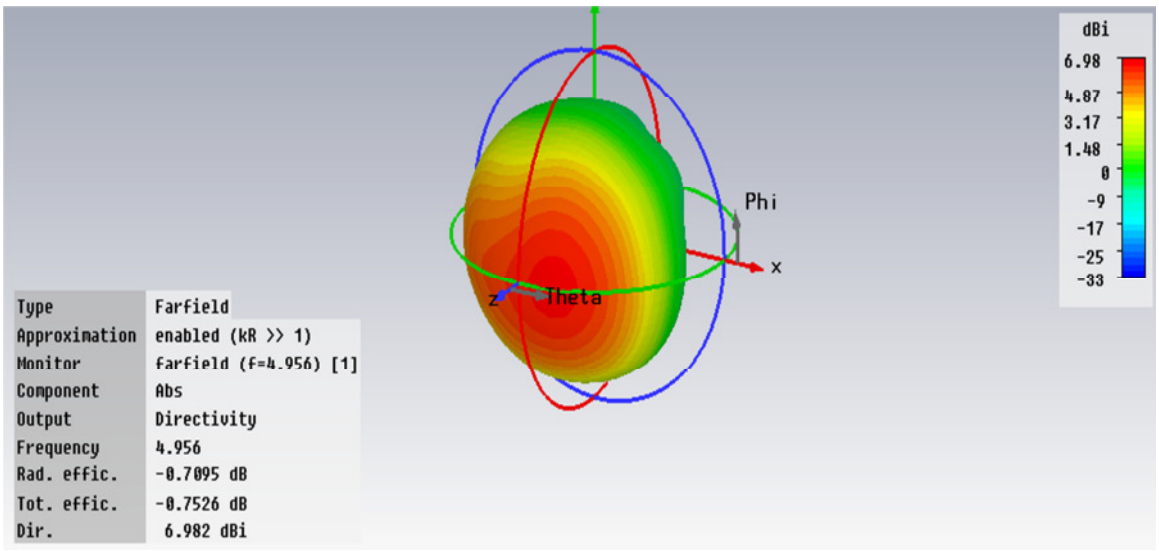

(b)

Figure 3.14. 3D plot for the simulated Design 2 at 4.956 GHz (a) Gain and (b) Directivity

- **E-field and H-field pattern:** The magnitude of main lobe of E-field is 12.6 dBV/m with angular width (3dB) of 90.4 deg. While the magnitude of main lobe of H-field is -30.9 dBA/m with angular width (3dB) of 80.9 deg. Figure 3.15. illustrates the E-field and H-field patterns.

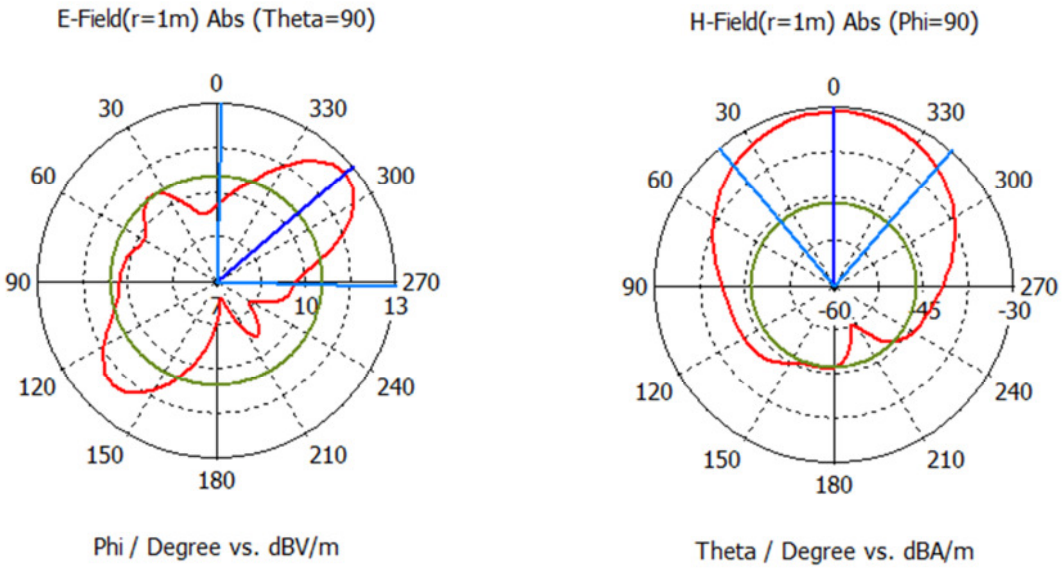

(a) **(b)**

Figure 3.15. Polar plot for the simulated Design 2 at 4.956 GHz (a) E-field pattern and (b) H-field pattern

- **Current Distribution:** The surface current distribution when coaxial feeding is provided at port1 has been shown in the Figure 3.16. The current is maximum at the center of the patch and minimum at edges as desired. Also, it has been observed that mutual coupling between the patches reduces as the slotted CSRR inclusion suppresses the electric fields normal to the ground plane and hence reduces the surface current flow to reach the patch of other antenna.

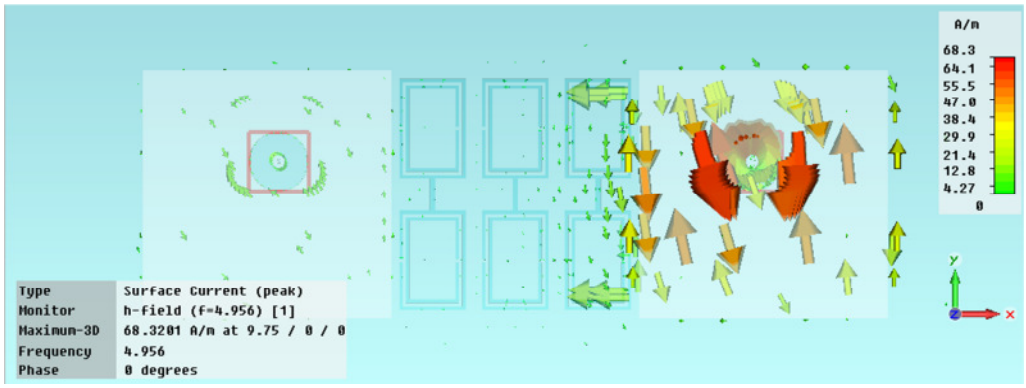

Figure 3.16. Surface current of the Design 2 at 4.956 GHz.

3.4. Conclusion:

- The simulated Design 1 for two identical coplanar rectangular MPAs resonates at 4.958 GHz while the simulated Design 2 with slotted CSRR structure has a resonant frequency of 4.956 GHz. Thus, the inclusion of slotted CSRR does not affect the resonant frequency of the patches.
- The simulated Design 1 exhibits the return loss of -26.0165 dB while Design 2 with slotted CSRR structure exhibits the return loss of -54.398 dB which shows significant reduction of return loss using metamaterial structure, that ultimately improve the quality of communication.
- The bandwidth attained through simulation of Design 1 for two identical coplanar rectangular MPAs is 97.5MHz while with Design 2 having slotted CSRR structure, bandwidth attained is 112.28MHz. Thus, improvement in bandwidth is achieved.
- The Slotted CSRRs reduce the mutual coupling between the two coplanar MPAs spaced by a quarter free-space wavelength as 2 dB reduction in the mutual coupling is observed when three Slotted CSRRs cells are placed in the ground plane between the patches. The reduction is possible because of the ability of the Slotted CSRRs to efficiently suppress the electric fields normal to the ground plane, which in turn reduces the surface currents in the terminated antenna element. The proposed structure can therefore be used to minimize coupling and co-channel interference in multiband antennas.

CHAPTER-4
DUAL-BAND RMPA WITH CSRRs FOR WLAN APPLICATIONS

4.1. Introduction

In this chapter a MPA consisting of two side-by-side CSRR structures on a single patch fed by a microstrip line has been been designed and simulated. The dual-bands have been attained due to the inductance produced by the current flowing along CSRR coils and the capacitances engendered by the voltage gradients between the CSRR gaps. The reduced ground structure has been employed to reduce harmonics. The suggested antenna covers WLAN 2.4/5.2 GHz wireless communication standards.

4.2. Antenna design

In order to attain the desired antenna performance, a set of parametric studies is done. The dimensions of the complementary ring elements as well as microstrip feed-line width have been varied for required resonant frequencies and return loss characteristics. Using CST Microwave Studio 2010, the design of the proposed antenna was simulated and the final dimensions of the antenna are shown in Table 4.1 (in millimetres):

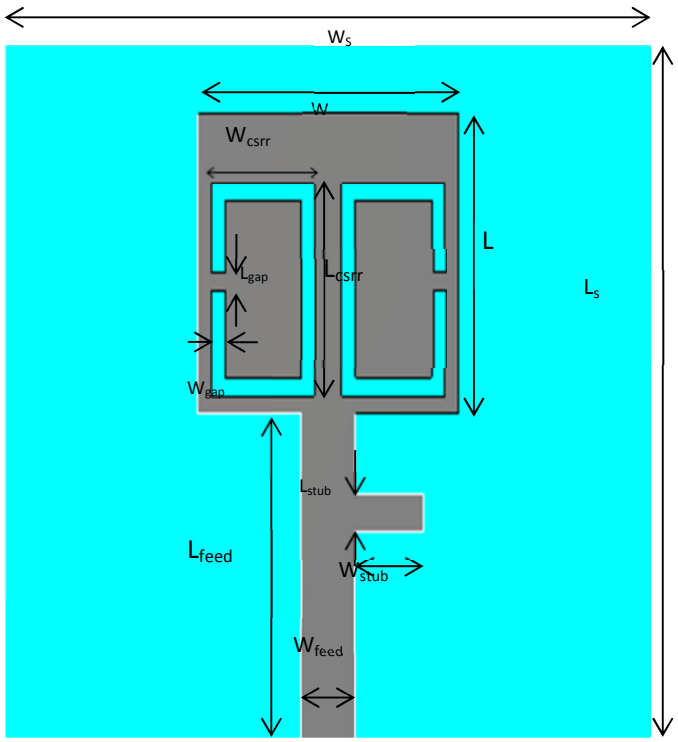

(a)

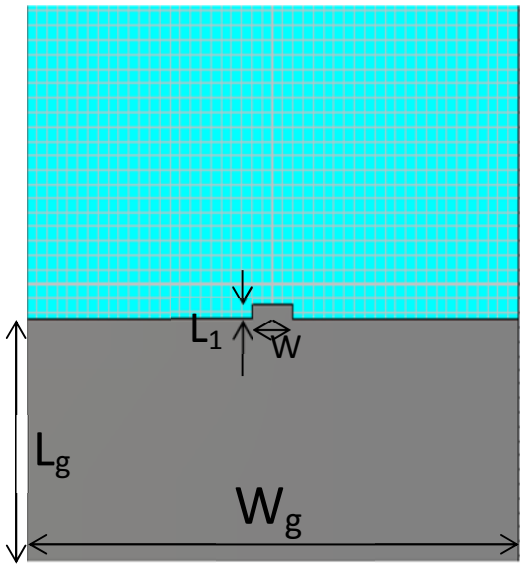

(b)

Figure 4.1. Simulated Design (a) Front View and (b) Back View

Table 4.1. Dimensions of the proposed antenna structure

Dielectric constant of substrate (ϵ_r)	4.4
Thickness of substrate(h)	1.57 mm
Length of substrate(L_s)	38.89 mm
Width of substrate(W_s)	47.88 mm
Length of patch(L)	16.73 mm
Length of ground(L_g)	18.44 mm
Width of ground(W_g)	47.88 mm
Length of Stub(L_{stub})	2 mm
Width of Stub(W_{stub})	5 mm
Length of CSRR ring (L_{csrr})	11.88 mm
Width of the ring(W_{csrr})	7.62 mm
Length of Split gap(L_{gap})	1 mm
Width of Split gap(W_{gap})	1 mm

4.2.1. Simulated results

- **Return Loss:** The proposed antenna attains dual resonant modes over the frequency ranges of 2.48 GHz and 5.30 GHz with reflection coefficient less than -10 dB as shown in Figure 4.2., thereby covering the two WLAN bands in 2.4 (2.4–2.484 GHz) and 5.2 (5.15–5.35 GHz) simultaneously according to IEEE standards. The bandwidth attained for these two bands is 340.24 MHz and 441.53 MHz respectively.

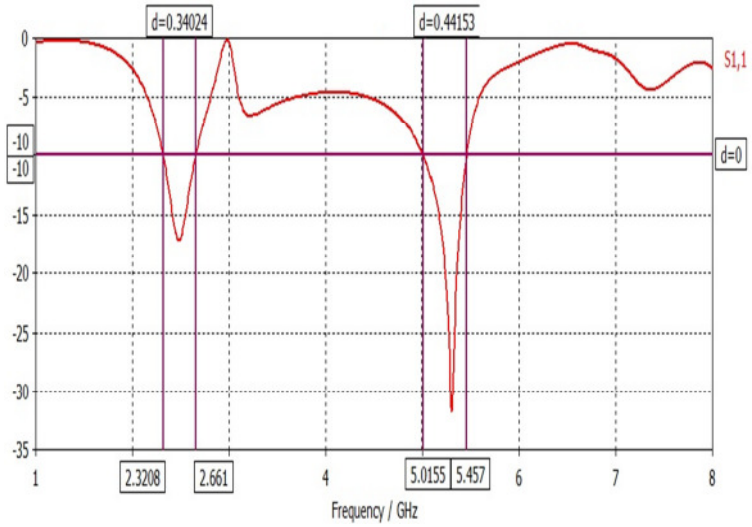

Figure 4.2. Plot of Return Loss vs. frequency

- **VSWR:** The VSWR vs. Frequency graph of the proposed antenna has been shown in Figure 4.3.which demonstrates that the VSWR value lies below 2 at both resonant frequencies as desired.

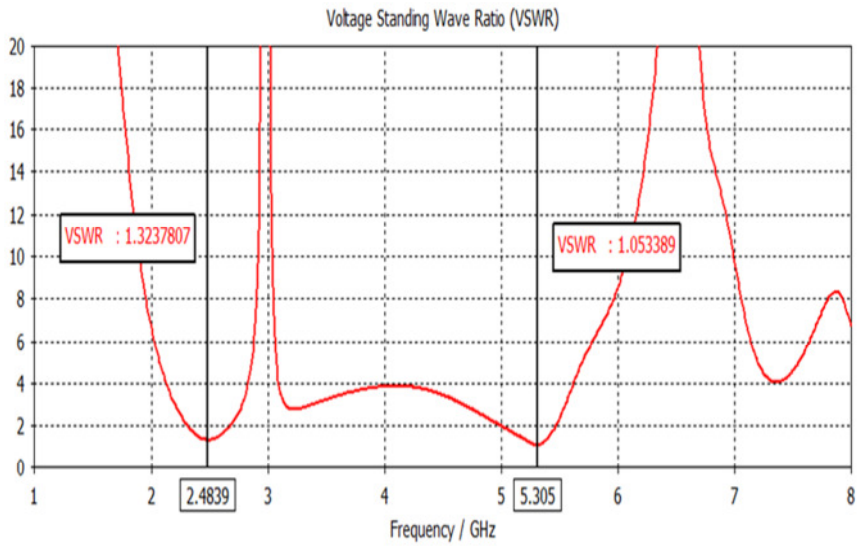

Figure 4.3. Plot of VSWR vs. frequency at 2.48 GHz and 5.305 GHz.

- **Gain and Directivity:** Gain is defined as the ratio of power radiated in a particular direction to the power radiated by an isotropic antenna. The 3D plot of gain is shown in Figure 4.4. which demonstrates that at resonating frequency of 2.483 GHz, the gain attained is 2.347 dB while at the resonating frequency of 5.30 GHz, the gain of the antenna comes out to be 2.876 dB.

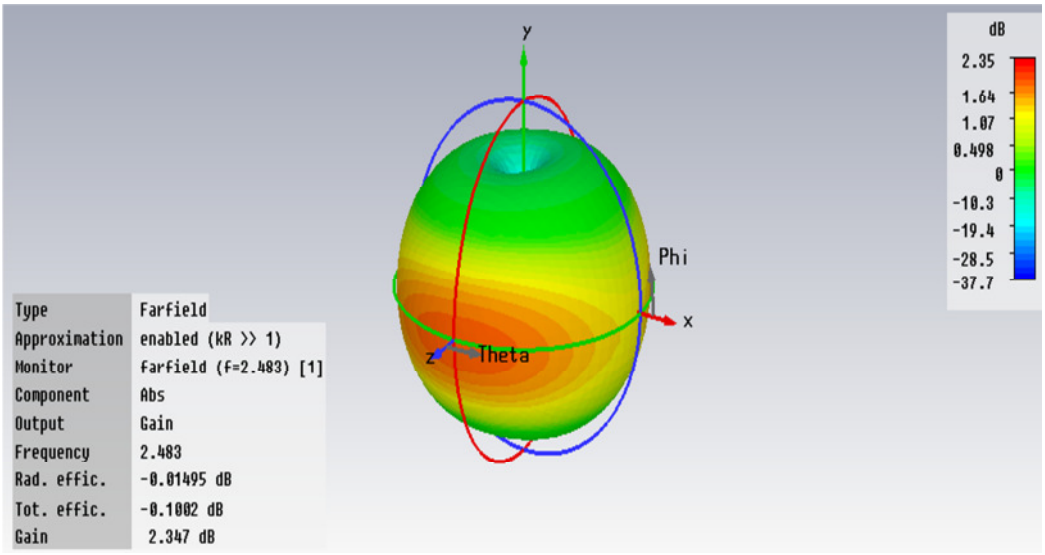

(a)

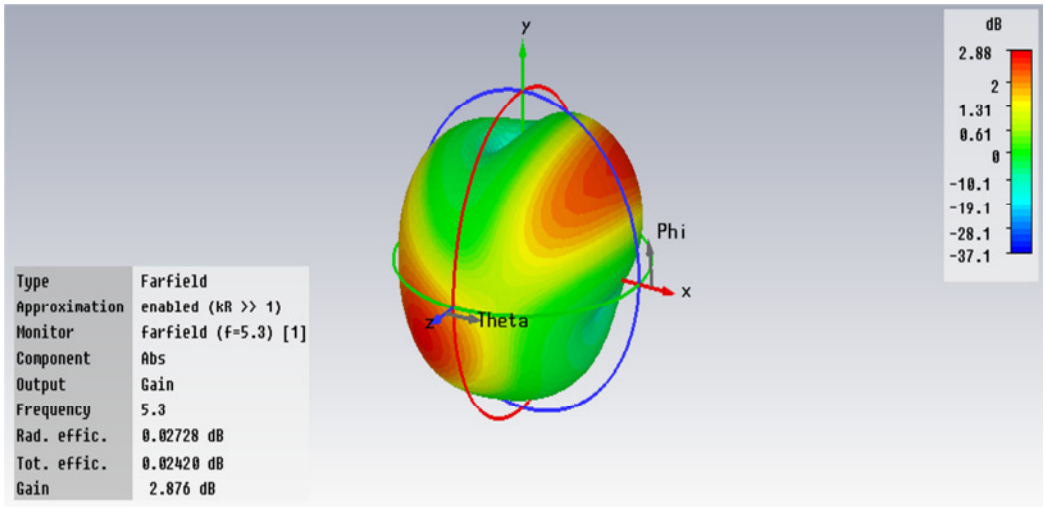

(b)

Figure 4.4. 3D- Plot for Gain at (a) 2.483 GHz and (b) 5.30 GHz

The 3D plot of directivity is shown in Figure 4.5. From the plot, the value of the directivity comes out to be 2.362 dBi at resonating frequency of 2.483 GHz while at the resonating frequency of 5.30 GHz, the value of the directivity comes out to be 2.849 dBi.

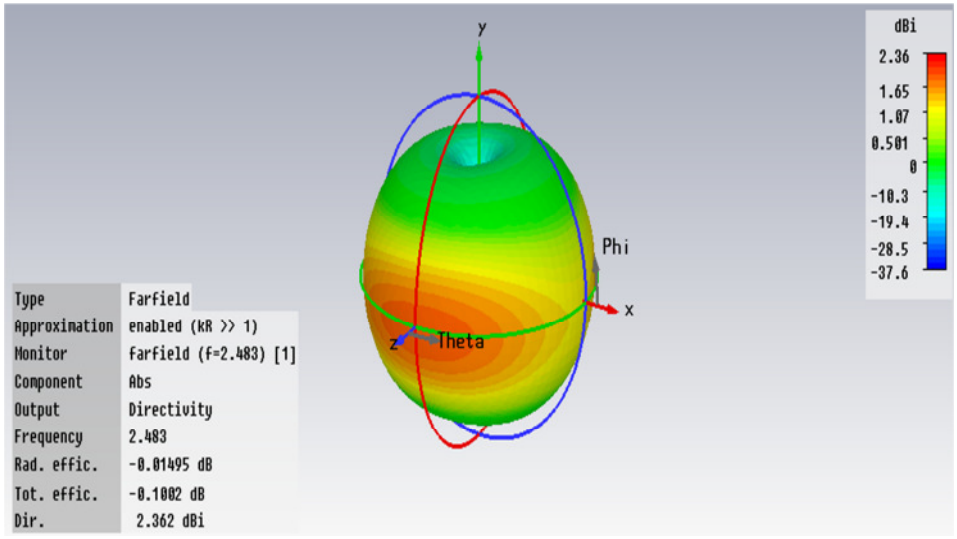

(a)

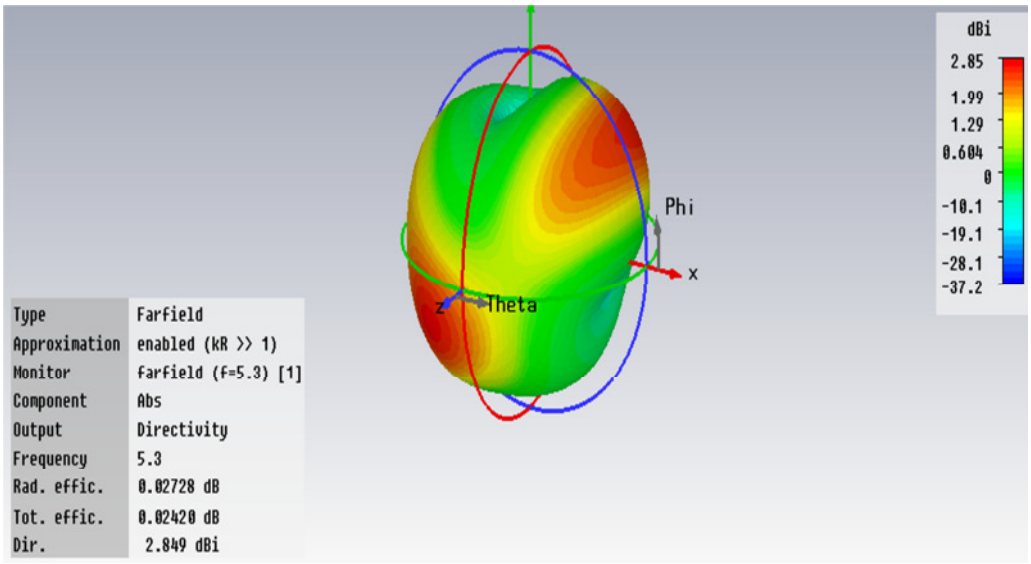

(b)

Figure 4.5. 3D- Plot for Directivity at (a) 2.483 GHz and (b) 5.30 GHz

- **E-field and H-field pattern:** The E-field pattern of the antenna at 2.483 GHz is shown in Figure 4.6.(a). The magnitude of the main lobe is 15.9 dBV/m which is directed at an angle of 356.0 deg. The half-power beamwidth (3dB) is 100.8 deg. The E-field pattern of the antenna at 5.30 GHz is shown in Figure 4.6.(b). The magnitude of the main lobe is 17.4 dBV/m which is directed at an angle of 40.0 deg. The half-power beamwidth (3dB) is 60.5 deg.

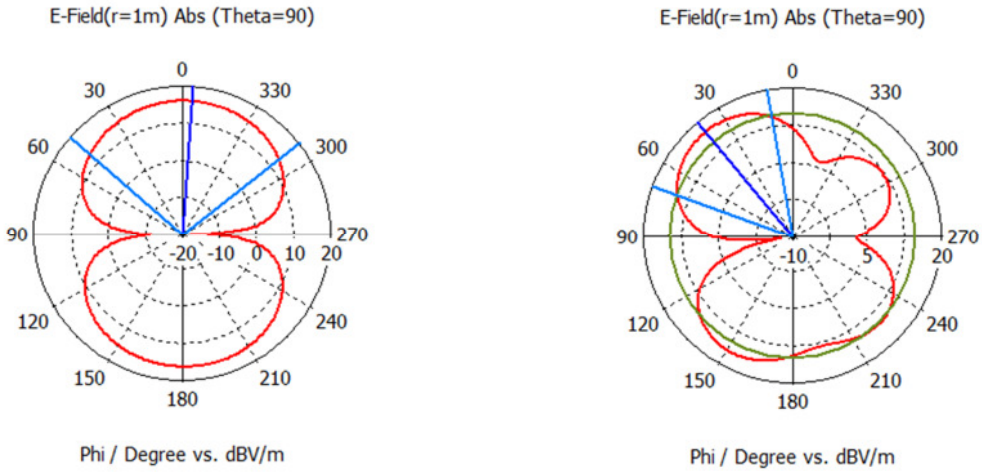

(a) **(b)**

Figure 4.6. E-field pattern at (a) 2.483 GHz and (b) 5.30 GHz

The H-field pattern of the antenna at 2.483 GHz is shown in Figure 4.7(a). The magnitude of the main lobe is -34.5 dBA/m which is directed at an angle of 181.0 deg.The half-power beamwidth (3dB) is 85.5 deg. The H-field pattern of the antenna at 5.30 GHz is shown in Figure 4.7.(b). The magnitude of the main lobe is -34.5 dBA/m which is directed at an angle of 344.0 deg. The half-power beamwidth (3dB) is 79.4 deg.

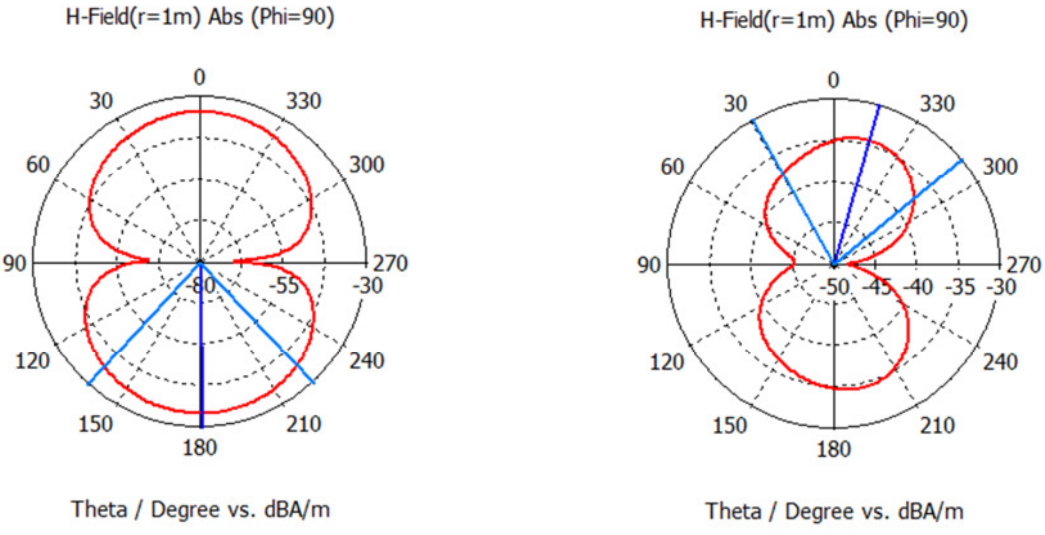

(a) **(b)**

Figure 4.7. H-field pattern at (a) 2.483 GHz and (b) 5.30 GHz

- **Current Distribution:** The surface current distribution of antenna has been shown in Figure 4.8. The current analysis demonstrates that at the two resonant frequencies, the

CSRR elements act as the main radiator of the antenna as the surface current flow mainly concentrates in the CSRR rings.

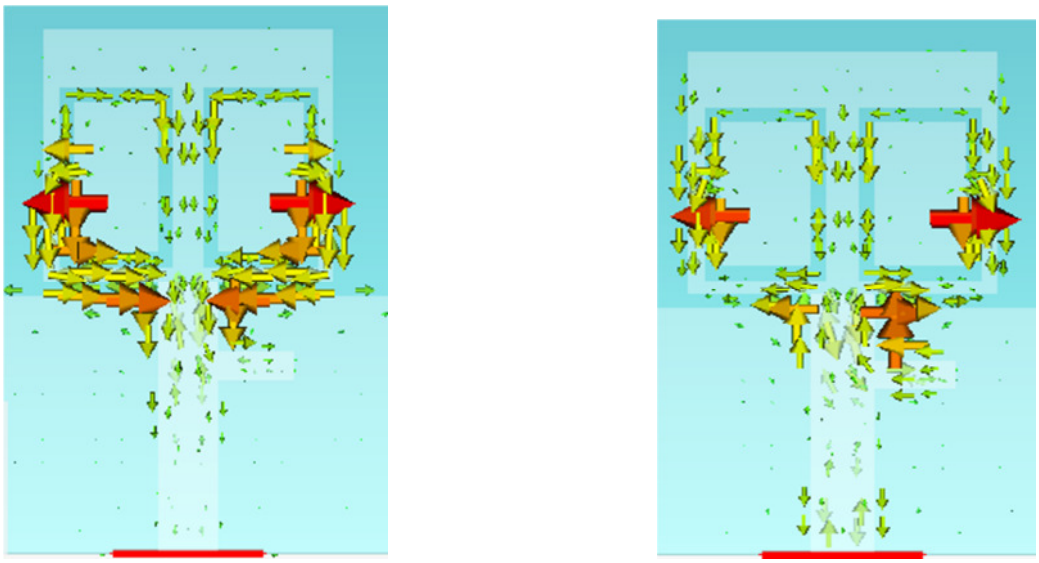

(a) (b)

Figure 4.8. Current density at (a) 2.48 GHz and (b) 5.30 GHz

4.3. Conclusion

The dual-band WLAN antenna with microstrip line feeding has been suggested in which complementary split-ring elements have been loaded on the patch. The simulated antenna performances obtained by CST Microwave Studio 2010 have been analysed. The compact antenna design resonates well at designated WLAN bands (2.4/5.2 GHz) with bandwidths of 340.24 MHz and 441.53MHz respectively. Also, VSWR achieved at both resonating frequencies are desirable. For further enhancement of the bandwidth and improvement in the return loss characteristics of MPA, different structures of CSRR can be designed. The antenna performance can also be investigated by incorporating different patch structures and feeding techniques.

CHAPTER-5
MULTI-BAND MPA WITH CSRRs FOR WIRELESS APPLICATIONS

5.1. Introduction

In this chapter, a multiband MPA which is based on complementary SRRs has been designed and simulated. The design consists of two side-by-side CSRR structures on a single patch fed by a microstrip line along with two open-circuited stubs that are added on each side of the antenna. The suggested antenna finds applications in various wireless systems since it covers different IEEE standards which include WLAN bands in 2.4 (2.4–2.484 GHz) and 5.8 (5.725–5.825 GHz), Bluetooth (2.4-2.5 GHz) and Wi-MAX bands of 2.5-2.69 GHz and 5.25-5.85 GHz and X-band satellite downlink (7.25 GHz-7.75 GHz).

5.2. Antenna design

The dimensions of patch, gound and substrate of the antenna have been calculated from the equations of Transmission Line Model as discussed in Chapter1. The desired antenna performance has been achieved by realizing a set of parametric studies. The dimensions of the complementary ring elements and have been varied for required resonant frequencies and return loss characteristics The simulated antenna design has been illustrated in Figure 5.1. and the final design specifications of the antenna are shown in Table 5.1 (in millimetres).

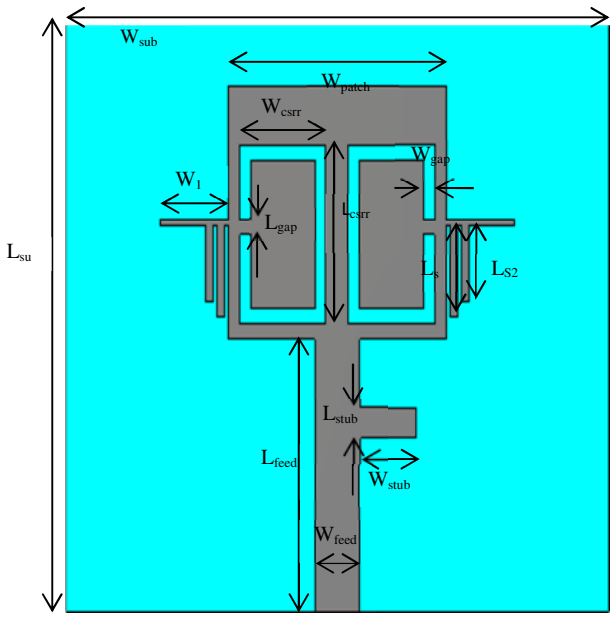

(a)

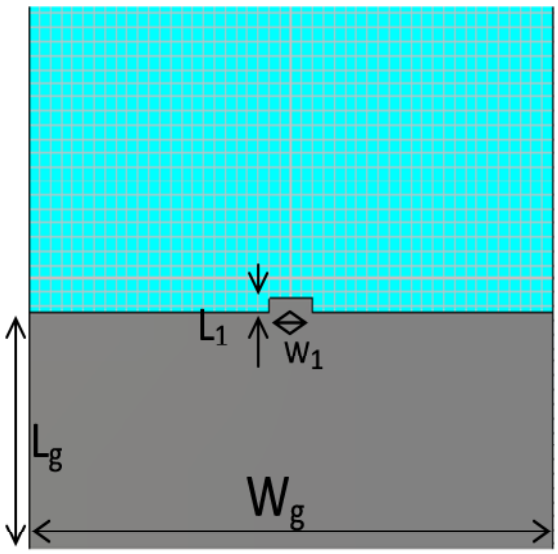

(b)

Figure 5.1. Simulated design (a) Front View and (b) Back view

Table 5.1. Design Specifications of the proposed antenna structure

Dielectric constant of substrate (ϵ_r)	4.4
Thickness of substrate(h)	1.57 mm
Length of substrate(L_s)	38.89 mm
Width of substrate(W_s)	47.88 mm
Width of patch(W_{patch})	19.24 mm
Length of ground(L_g)	18.44 mm
Width of ground(W_g)	47.88 mm
Length of Stub(L_{stub})	2 mm
Width of Stub(W_{stub})	5 mm
Length of CSRR ring (L_{csrr})	11.88 mm
Width of the ring(W_{csrr})	7.62 mm
Length of Split gap(L_{gap})	1 mm
Width of Split gap(W_{gap})	1 mm
Length of stub1(L_{s1})	6 mm
Length of stub2(L_{s2})	5 mm

5.2.1. Simulated results

- **Return Loss:** The proposed antenna has achieved multiple resonant modes with reflection coefficient of less than -10 dB over the frequency ranges of 2.449 GHz, 5.844 GHz and 7.398 GHz as shown in Figure 5.2. The bandwidth attained over these bands is 267.9 MHz, 204.5 MHz and 97.2 MHz respectively. Thus, various wireless standards that have been covered include the two WLAN bands in 2.4 (2.4–2.484 GHz) and 5.8 (5.725–5.825 GHz), Bluetooth (2.4-2.5 GHz) and Wi-MAX bands of 2.5-2.69 GHz and 5.25-5.85 GHz and satellite downlink band of 7.25-7.75 GHz according to IEEE standards.

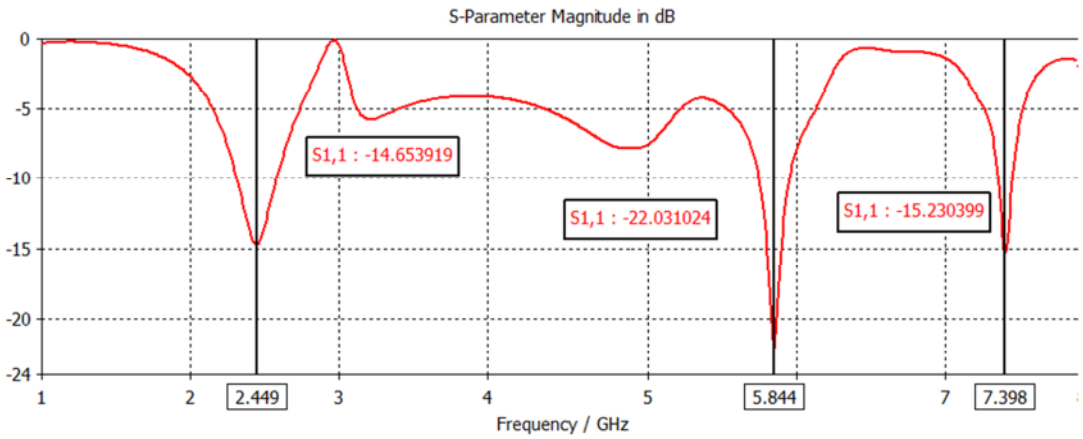

Figure 5.2. Plot of Return Loss vs. frequency

- **VSWR:** The VSWR vs. Frequency graph of the proposed antenna has been shown in Figure 5.3 which demonstrates that the VSWR value lies below 2 at both resonant frequencies as desired.

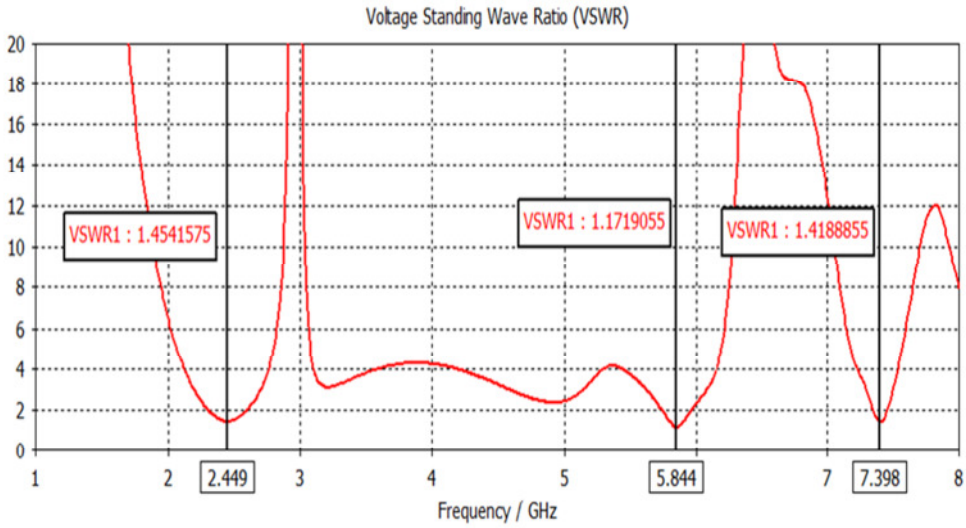

Figure 5.3. Plot of VSWR vs. frequency at 2.449 GHz, 5.844 GHz and 7.398 GHz.

- **Gain and Directivity:** The 3D plot of gain is shown in Figure 4.4. which demonstrates that at resonating frequency of 2.449 GHz, the gain attained is 2.478 dB while at the resonating frequency of 5.844 GHz, the gain of the antenna comes out to be 5.069 dB. The value of gain achieved at resonating frequency of 7.398 GHz comes out to be 5.395 dB.

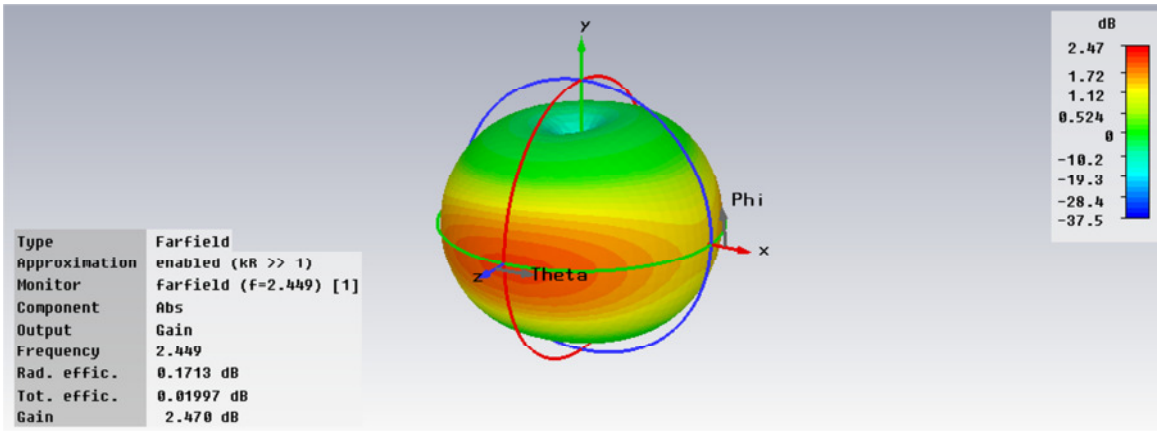

(a)

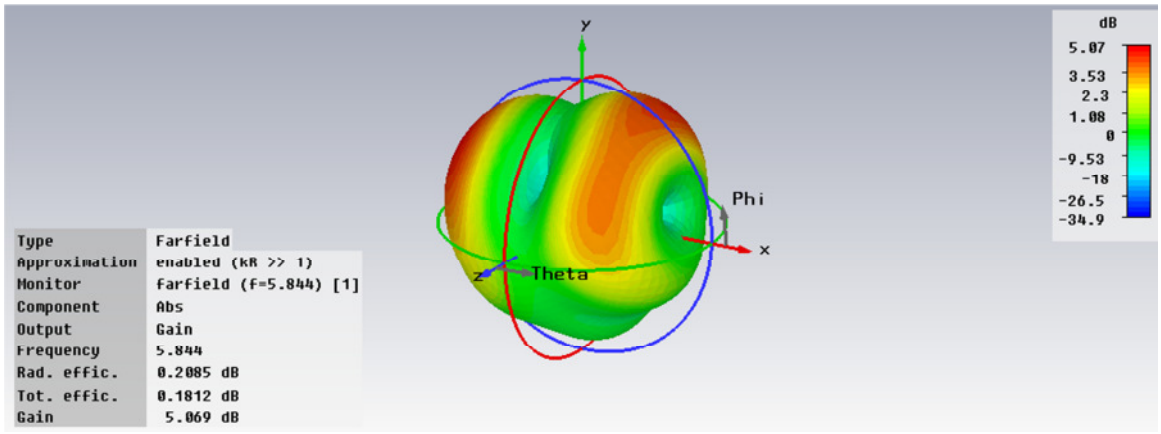

(b)

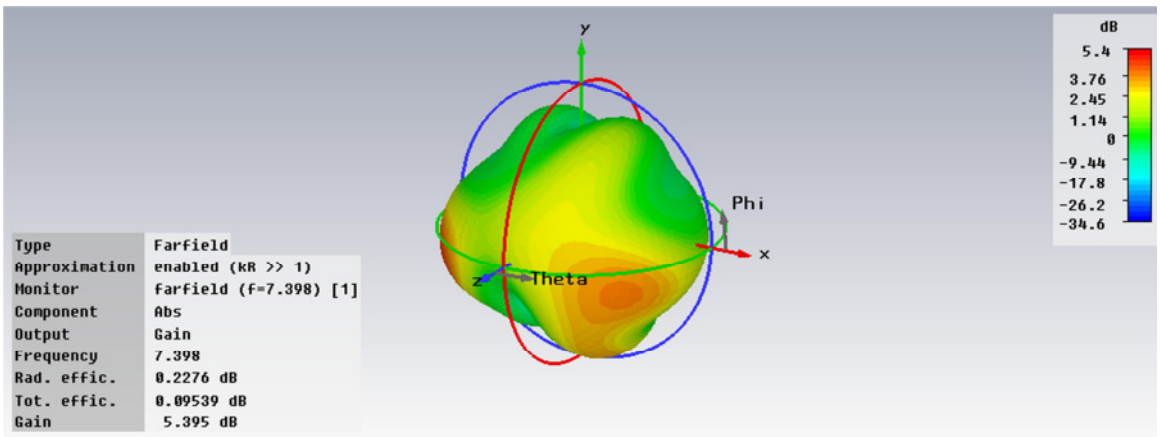

(c)

Figure 5.4. 3D-plot of Gain at (a) 2.449 GHz, (b) 5.844 GHz and (c) 7.398 GHz

The 3D plot of directivity is shown in Figure 5.5. From the plot, the value of the directivity comes out to be 2.298 dBi at resonating frequency of 2.449 GHz while at the resonating frequency of 5.844 GHz, the value of the directivity comes out to be 4.868 dBi. The value of directivity at resonating frequency of 7.398 GHz comes out to be 5.168 dBi.

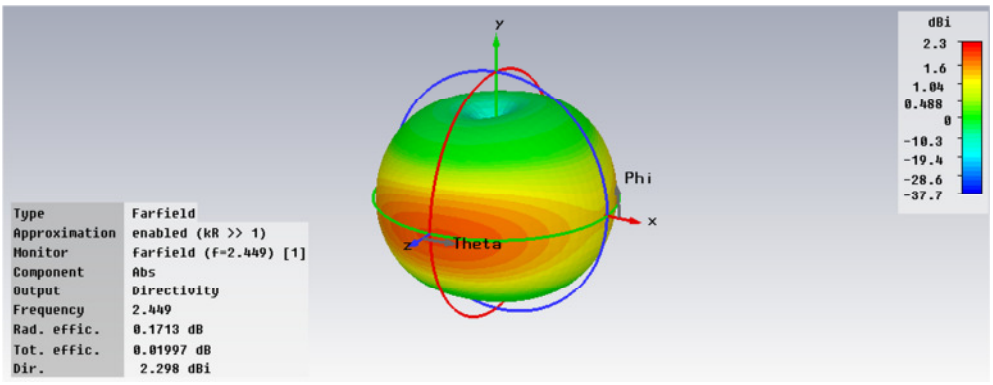

(a)

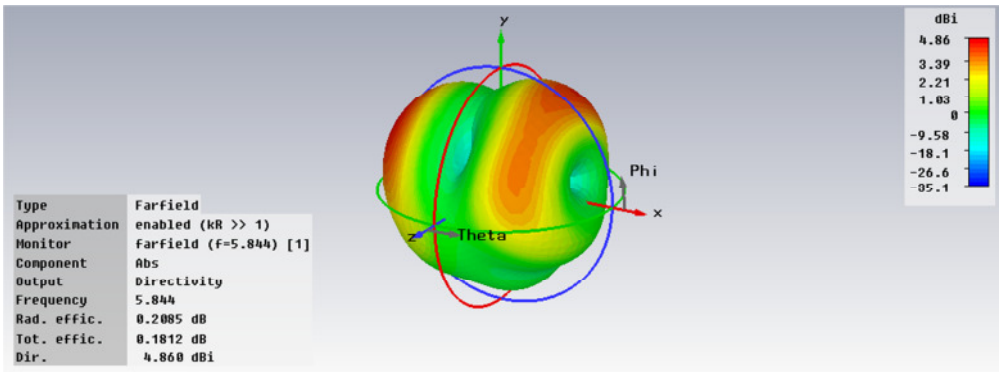

(b)

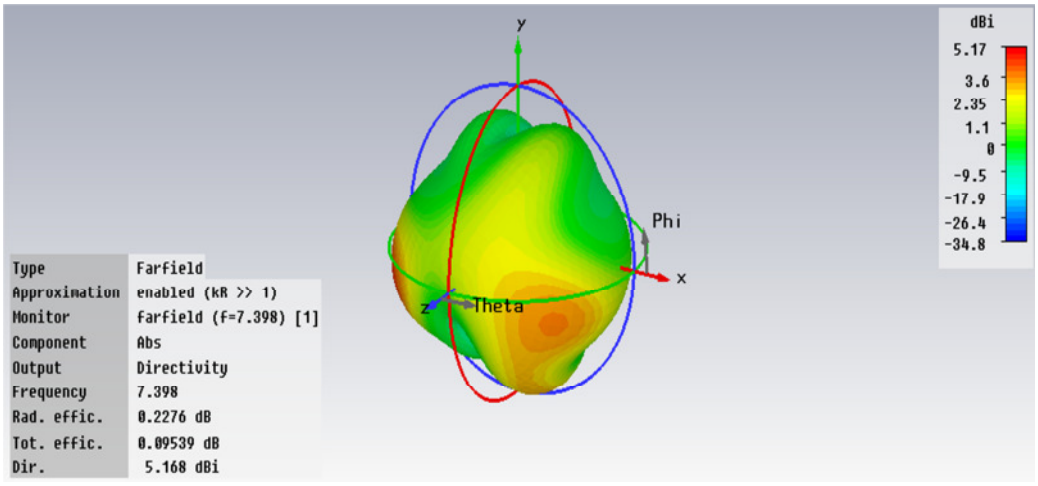

(c)

Figure 5.5. 3D- plot for Directivity at (a) 2.449 GHz, (b) 5.844 GHz and (c) 7.398 GHz

- **E-field and H-field pattern**: The E-field pattern of the antenna at 2.449 GHz is shown in Figure 5.6 (a). The magnitude of the main lobe is 16 dBV/m which is directed at an angle of 359.0 deg. The half-power beamwidth (3dB) is 104.5 deg. The E-field pattern of the antenna at resonating frequency of 5.844 GHz is shown in Figure 5.6(b). The magnitude of the main lobe is 19.4 dBV/m with half-power beamwidth (3dB) of 52.6 deg. The E-field pattern of the antenna at 7.398 GHz is shown in Figure 5.6.(c). The magnitude of the main lobe is 19.7 dBV/m. The angular width (3dB) comes out to be 47.3 deg.

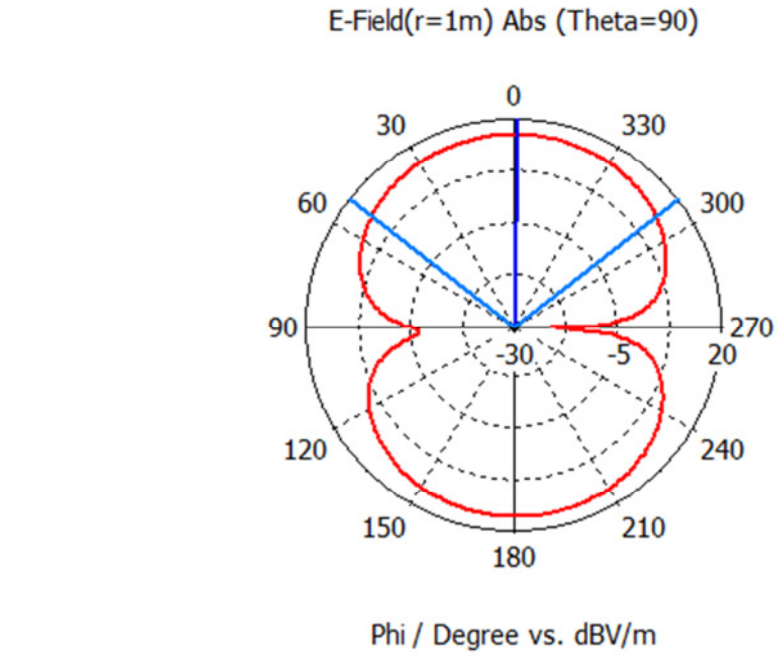

(a)

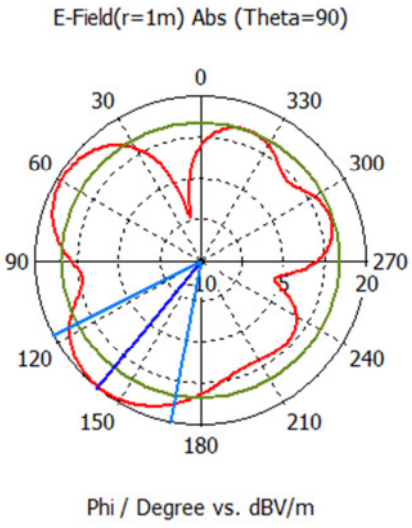

(b)

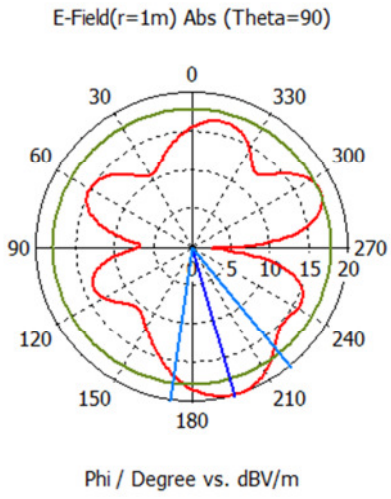

(c)

Figure 5.6. E-field pattern at (a) 2.449 GHz, (b) 5.844 GHz and (c) 7.398 GHz

The H-field pattern of the antenna at resonating frequency of 2.449 GHz is shown in Figure 5.7(a). The magnitude of the main lobe is -34.4 dBA/m which is directed at an angle of 180.0 deg. The half-power beamwidth (3dB) is 85.8 deg. The H-field pattern of the antenna at 5.844 GHz is shown in Figure 5.7(b). The magnitude of the main lobe is -37.0 dBA/m with half-power beamwidth (3dB) of 78.3 deg. The H-field pattern of the antenna at resonating frequency of 7.398 GHz is shown in Figure 5.7(c). The magnitude of the main lobe is -34.7 dBA/m and the angular width (3dB) comes out to be 72.5 deg.

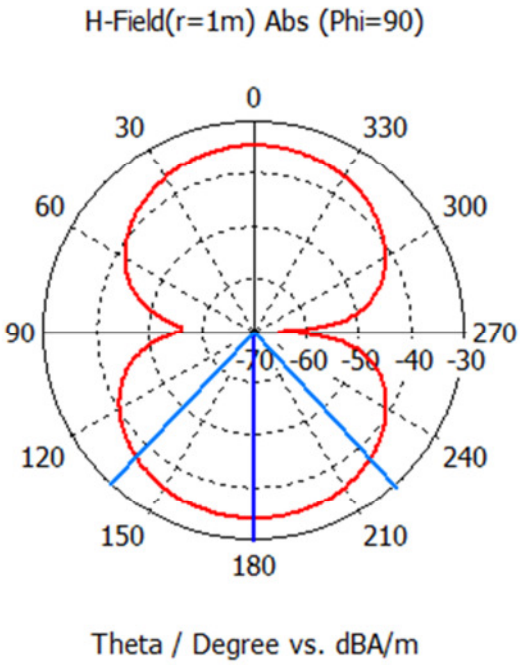

(a)

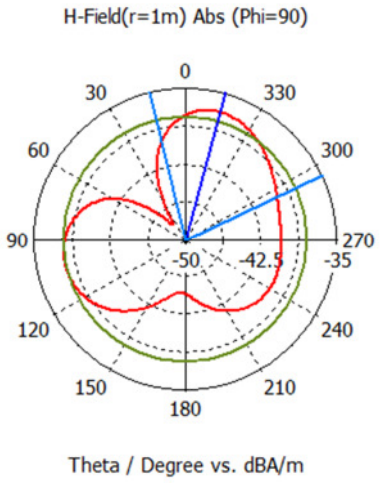

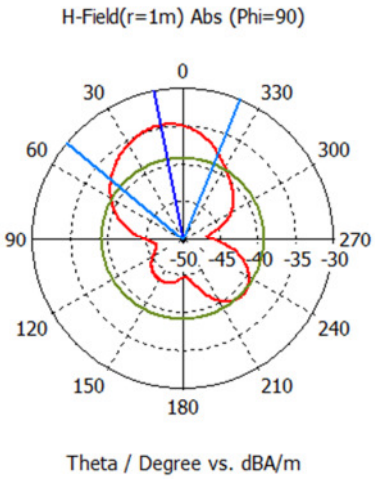

(b) **(c)**

Figure 5.7. H-field pattern at (a) 2.449 GHz, (b) 5.844 GHz and (c) 7.398 GHz

- **Current Distribution:** The surface current distribution at the three resonant frequencies have been shown in Figure 5.8. Current analysis of antenna demonstrates that at the resonating frequency of 2.449 GHz, the CSRR elements act as the main radiator of the antenna as the surface current flow mainly concentrates in the CSRR rings. While at resonant frequencies of 5.844GHz and 7.398GHz, the current mainly flows through the two stubs that are added on both sides of antenna.

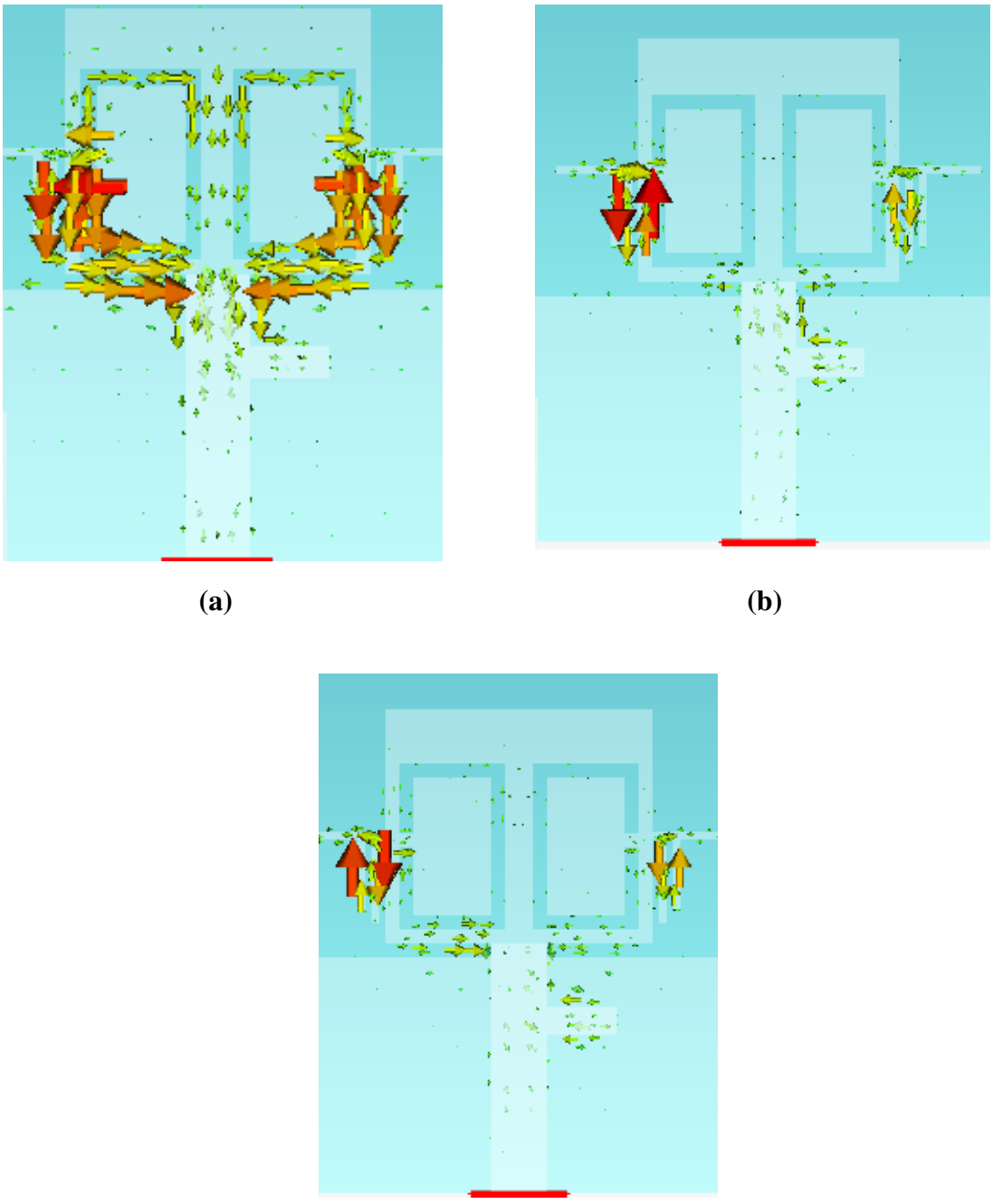

(a) **(b)**

(c)

Figure 5.8. Current density at (a) 2.449 GHz, (b) 5.844 GHz and (c) 7.398 GHz.

5.3. Fabrication and Measurement

The fabrication multiband MPA with CSRR and stub loading has been illustrated in Figure 5.9. The material used for fabrication of antenna is PEC (copper) of height 0.02 mm with FR4 substrate of dielectric constant 4.4 and thickness 1.57 mm.

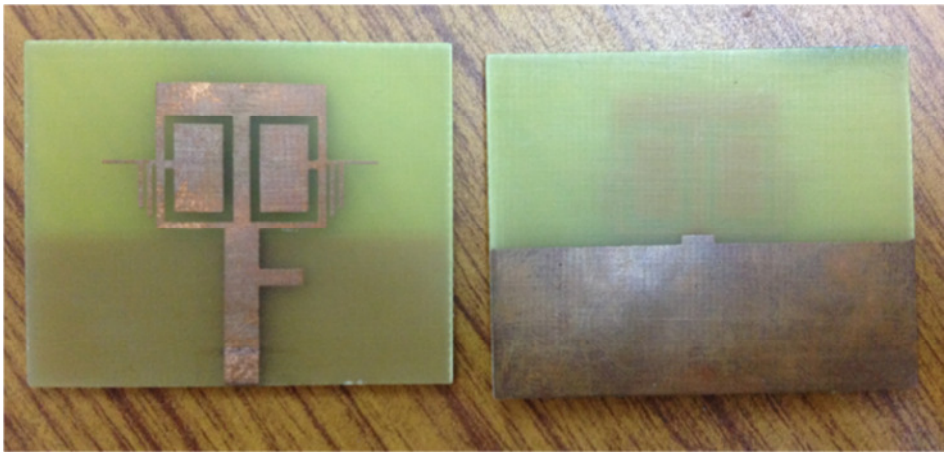

Figure. 5.9. Top view and Back view of the fabricated antenna

The testing of the antenna is done using VNA (Vector Network Analyser).

Figure. 5.10. Vector Network Analyser for testing

5.4. Comparison of Simulated and Measured results

The simulated results and the measured results of the fabricated antenna have been illustrated in Figure 5.11. The fabricated antenna has shown results that approximately matched with the simulated results. However, the band with the resonant frequency of 7.398 GHz obtained in the simulated results goes missing in the measured results which might be due to fabrication and testing errors or a consequence of noise or interference.

Table 5.2 shows comparison between simulated and measured results in terms of return loss, resonant frequency and bandwidth.

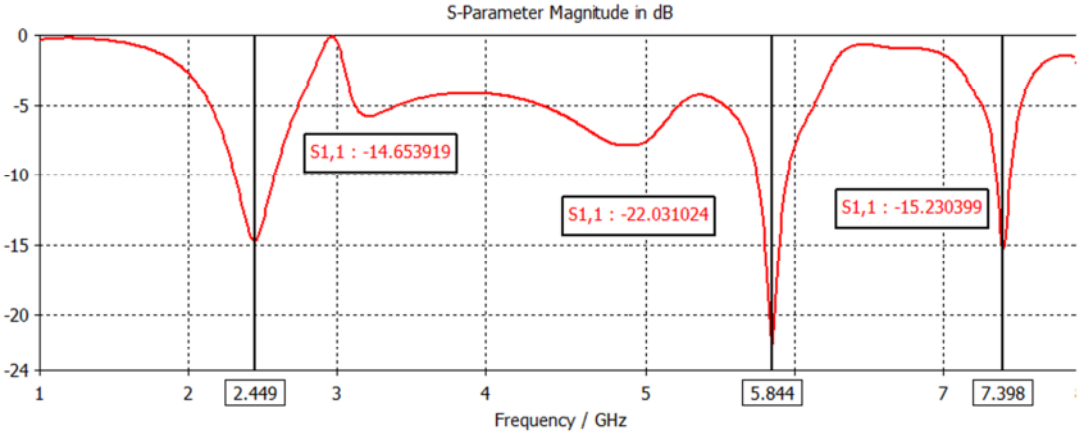

(a)

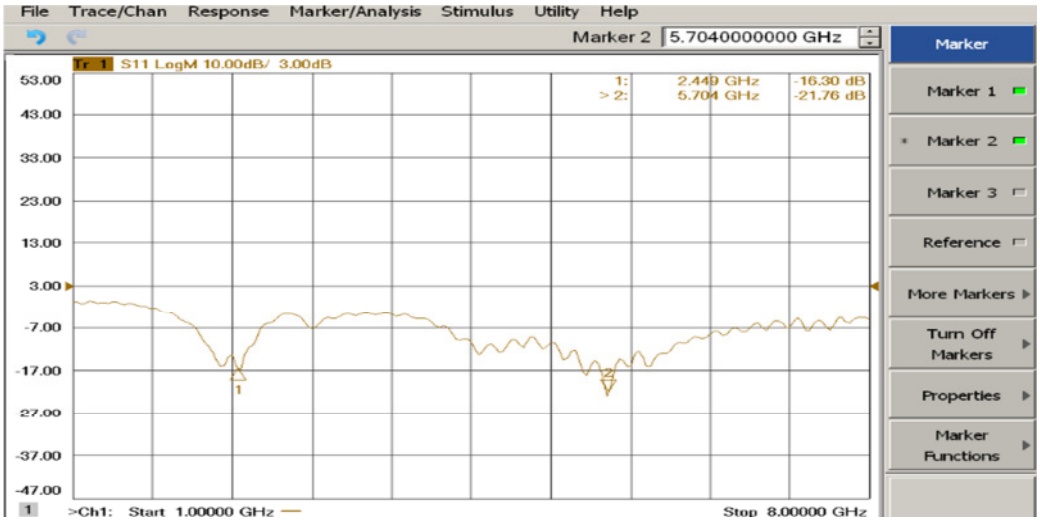

(b)

Figure 5.11. Return Loss (a) Simulated results and (b) Measured results

Table 5.2. Comparison of Simulated and Measured Results

Parameters	**Simulated results at 2.4 GHz**	**Measured results at 2.4 GHz**	**Simulated results at 5.8 GHz**	**Measured results at 5.8 GHz**
Return Loss	-14.65 dB	-16.30 dB	-22.03 dB	-21.76 dB
Resonant frequency	2.449 GHz	2.449 GHz	5.844 GHz	5.704 GHz
Bandwidth	267.9 MHz	255 MHz	204.5MHz	200 MHz

CHAPTER-6
CONCLUSION AND FUTURE SCOPE

6.1. Conclusion

This chapter sums up all the work presented in this thesis, and then obtains a conclusion that would help in the development of this work and finally present the future work.

Firstly, two designs, one having two coplanar rectangular MPAs without slotted CSRR while other with slotted CSRR in the ground plane have been simulated. The simulation results confirm that the presence of slotted CSRR shows significant reduction of return loss along with improvement in the bandwidth. In addition, reduction in the mutual coupling between two antenna elements has been observed.

Further, a microstrip-fed dual band antenna with complementary SRR loading on the patch has been designed which covers 2.4/5.2 GHz WLAN standard. The obtained -10 dB impedance bandwidth for this antenna is 340.24 MHz and 441.53 MHz at the bands of 2.48 GHz and 5.30 GHz respectively.

This antenna design is further modified to a multiband MPA consisting of two open-circuited stubs added on each side of the antenna along with two side-by-side CSRR structures over a single patch has been designed and simulated which covers WLAN bands in 2.4 (2.4–2.484 GHz) and 5.8 (5.725–5.825 GHz), Bluetooth (2.4-2.5 GHz) and Wi-MAX bands of 2.5-2.69 GHz and 5.25-5.85 GHz and X-band satellite downlink (7.25 GHz-7.75 GHz). The obtained -10 dB impedance bandwidth are 267.9 MHz, 204.5 MHz and 97.2 MHz over the resonating frequency ranges of 2.449 GHz, 5.844GHz and 7.398 GHz respectively. Also, the antenna gains achieved at these three bands are 2.478 dB, 5.069 dB and 5.395dB respectively.

Finally, this multiband antenna has been fabricated using PCB technology and tested on VNA. The comparison between simulated results and measured results has been analysed.

6.2. Future Scope

- In this thesis, optimization of parameters has been done manually. One can use inbuilt optimizer to optimize the parameters using optimization techniques. One can optimize the parameters via. writing the program using MATLAB to optimize the various parameters, then calibrating MATLAB with CST.

- The proposed dual band MPA has small value of gain and it can be enhanced by using photogenic band gap (PBG).
- EBG (Electromagnetic Band Gap) substrates have been found to reduce the effect of surface waves which is a function of frequency. Moreover, these structures provide performance of a broadband frequency. Hence, CSRR based MPAs incorporating EBG can be designed.
- For the enhancement of the bandwidth and improvement in the return loss characteristics of MPA, different structures of CSRR can be designed. The antenna performance can also be investigated by incorporating different patch structures and feeding techniques.
- Wideband and ultra-wideband patch antenna can be designed which is helpful in telecommunication and high speed data transmission systems.

REFERENCES

[1] http:en.wiki .edia.org/wiki/Wimax/Wlan.

[2] A. B. Mutiara, R. Refianti, and Rachmansyah, "Design of microstrip patch antenna for wireless communication at 2.4 GHz," *Journal of Theoretical and Applied Information Technology*, vol. 33, no.2, 2011.

[3] P. Bhartia, I. Bahl, R. Garg, and A. Ittipiboon, "Microstrip Patch Antenna Design Handbook," *Artech House Antennas and Propagation Library*, 2000.

[4] C. A. Balanis, "Antenna Theory, Analysis and Design," *John Wiley & Sons*, New York, 1997.

[5] T. Narangi and S. Jain, "Microstrip Patch Antenna - A Historical Perspective of the Development," *Conference on Advances in Communication and Control Systems,* 2013.

[6] S. A. Ramakrishna, "Physics of negative refractive index materials," *Rep. Prog. Phys*., vol. 68, pp. 449-521, 2005.

[7] V.G. Veselago, "The electrodynamics of substances with simultaneously negative values of ε and μ," *Soviet Physics Uspekhi*, vol. 10, no. 4, pp. 509–514, 1968.

[8] D. M. Pozar, "Microwave Engineering 3rd edition," *John Wiley & Sons*, 2005.

[9] M. C. K. Wiltshire, "Bending of light in the wrong way," *Science*, vol. 292, no. 5514, pp. 60-61, 2001.

[10] S. A. Schelkunoff, and H. T. Friss, "Antennas: Theory and Practice," *John Wiley & Sons*, New York, 1952.

[11] F. Falcone, T. Lopetegi, M. A. G. Laso, J. D. Baena, J. Bonache, M. Beruete, R. Marques, F. Martin, and M. Sorolla, "Babinet Principle Applied to the Design of Metasurfaces and Metamaterials," *Phys. Rev. Lett.*, vol. 93, no. 19, 2004.

[12] J. B. Pendry, A. J. Holden, D. J. Robbins, and W. J. Stewart, "Magnetism from conductors and enhanced nonlinear phenomena," *IEEE Transactions on Microwave Theory and Techniques*, vol. 47, pp. 2075-2084, 1999.

[13] J. D. Jackson, "Classical Electrodynamics 3rd edition," Wiley, 1999.

[14] V. Rajeshkumar, and S. Raghavan, "A compact CSRR loaded dual band MPA for wireless applications," *IEEE International conference on Computational Intelligence and Computing Research*, pp. 1-4, 2013

[15] I. B. Issa, and M. Essaaidi, "Compact Multi-Band Square Complementary SRR Patch Antenna For Wireless Applications," *Mediterranean Microwave Symposium*, pp.1-4, 2013.

[16] M. M Bait-Suwailam, and H. M. AI-Rizzo, "Size Reduction of Microstrip Patch Antennas Using Slotted Complementary Split-Ring Resonators," *International Conference on Technological Advances in Electrical, Electronics and Computer Engineering*, pp. 528-531, 2013.

[17] S. C. Basaran, U. Olgun, and K. Sertel, "Multiband monopole antenna with complementary split-ring resonators for WLAN and WiMAX applications," *Electronics Letters*, vol. 49, no. 10, 2013.

[18] M. U. Vakani, K. H. Wandra, and A. K. Sarvaiya, "Comparative Analysis of Small Size Dual Band SRR Based Antenna," *Nirma University International Conference on Engineering*, pp.1-4, 2012.

[19] S. C. Basaran, "A compact dual-wideband antenna based on complementary split-ring resonator," *Microwave and Optical Technology Letters*, vol. 54, no.8, pp. 1917–1919, 2012.

[20] Y. Dong, H. Toyao, and T. Itoh, "Design and Characterization of Miniaturized Patch Antennas Loaded With Complementary Split-Ring Resonators," *IEEE Transactions on Antennas and Propagation*, vol.60, no.2, pp.772-785, 2012

[21] W. Cao, Y. Xiang, B. Zhang, A. Liu, T. Yu, and D. Guo, "A Low-Cost Compact Patch Antenna With Beam Steering Based on CSRR-Loaded Ground," *IEEE Antennas and Wireless Propagation Letters*, vol.10, pp.1520-1523, 2011.

[22] X. Cheng, D. E. Senior, C. Kim, and Yong-Kyu Yoon, "A Compact Omnidirectional Self-Packaged Patch Antenna With Complementary Split-Ring Resonator Loading for Wireless Endoscope Applications," *IEEE Antennas and Wireless Propagation Letters*, vol.10, pp.1532-1535, 2011.

[23] Ó. Quevedo-Teruel , M. N. MouKehn, and E. Rajo-Iglesias, "Dual-Band Patch Antennas Based on Short-Circuited Split Ring Resonators," *IEEE Transactions on Antennas and Propagation*, vol. 59, no. 8, pp. 2758-2765, 2011.

[24] N. Ortiz, F. Falcone, and M. Sorolla, "Radiation Efficiency Improvement of Dual Band Patch Antenna Based on Complementary Rectangular Split Ring Resonators," *Proceedings of 5th European Conference on Antenna and Propagation*, pp. 830-834, 2011.

[25] S. S. Pattnaik, J. G. Joshi, S. Devi, and M. R. Lohokare, "Electrically Small Rectangular Microstrip Patch Antenna Loaded with Metamaterial," *International Symposium on Antennas Propagation and EM Theory*, pp. 247-250, 2010.

[26] L. Ke, W. Guang-Ming, X. Tong, and X. He-Xiu, "A Novel Circularly Polarized Antenna Based on the Single Complementary Split Ring Resonator," *International Symposium on Signals Systems and Electronics*, vol. 2, pp. 1-4, 2010.

[27] M. M. Bait-Suwailam, O. F. Siddiqu, and O. M. Ramahi, "Mutual Coupling Reduction between Microstrip Patch Antennas Using Slotted-Complementary Split-Ring Resonators," *IEEE Antennas and Wireless propagation Letters*, vol. 9, pp. 876-878, 2010.

[28] J. J. Ma, X. Y. Cao, and T. Liu, "Design the Size Reduction Patch Antenna Based on Complementary Split Ring Resonators," *International Conference on Microwave and Millimeter Waver Technology*, pp. 401-402, 2010.

[29] C. J. Sanchez-Femandez, O. Quevedo-Teruel, J. RequenaCarrion, L. Inclan-Sanchez, E. Rajo-Iglesias, and M. N. Moukehn, "Dual-Band Implantable Antenna Based on Short-Circuited Split Ring Resonator," *Proceedings of the Fourth European Conference on Antenna and Propagation*, pp. 1-4, 2010.

[30] N. Ortiz, F. Falcone, and M. Sorolla, "Dual band patch antenna based on Complementary Rectangular Split-Ring Resonators," *Microwave Conference*, pp. 2762-2765, 2009.

[31] S. R. BhadraChoudhuri, D. R. Poddar, R. Ghatak, and R. K. Mishra, "Modulating Properties of a Microstrip Patch Antenna Using Complementary Split Ring Resonator," *IEEE International Workshop on Antenna Technology*, pp.1-4, 2009.

[32] H. Zhang, You-Quan Li, X. Chen, Yun-Qi Fu, and Nai-Chang Yuan, "Design of Circular Polarization Microstrip Patch Antennas with Complementary Split Ring Resonator," *International Workshop on Metamaterials*, pp. 360-362, 2008.

[33] R. Karimzadeh Baeel, G. Dadashzadehl, and F. Geran Kharakhilil, "Using of CSRR and its Equivalent Circuit Model in Size Reduction of Microstrip Patch Antenna," *Microwave Conference*, pp. 1-4, 2007.

[34] A. U. Limaye, and J. Venkataraman "Size Reduction in Microstrip Patch Antennas using Left-Handed Materials Realized by Complementary Split-Ring

Resonators in Ground Plane," *International Symposium on Antennas and Propagation Society*, pp. 1869-1872, 2007.

[35] Y. Lee, S. Tse, Y. Hao, and C. G. Parini, "A Compact Microstrip Antenna with Improved Bandwidth Using Complementary Split-Ring Resonator (CSRR) Loading," *International Symposium on Antennas and Propagation Society*, pp. 5431- 5434, 2007.

[36] J. D. Baena, J. Bonache, F. Martín, R. M. Sillero, F. Falcone, T. Lopetegi, M. A. G. Laso, J. García–García, I. Gil, M. F. Portillo, and M. Sorolla, "Equivalent-Circuit Models for Split-Ring Resonators and Complementary Split-Ring Resonators Coupled to Planar Transmission Lines," *IEEE Transactions On Microwave Theory And Techniques*, vol. 53, no. 4, 2005.

PUBLICATION

Smriti and Jaswinder Kaur, "Complementary Split-Ring Resonators based Dual-Band microstrip patch antenna for WLAN Applications," IJARCCE, vol. 3, no. 5, May 2014.